



## Near-infrared transmission spectrum of TRAPPIST-1 h using Hubble WFC3 G141 observations

Amélie Gressier, M. Mori, Q. Changeat, B. Edwards, J.-P. Beaulieu,  
Emmanuel Marcq, Benjamin Charnay

### ► To cite this version:

Amélie Gressier, M. Mori, Q. Changeat, B. Edwards, J.-P. Beaulieu, et al.. Near-infrared transmission spectrum of TRAPPIST-1 h using Hubble WFC3 G141 observations. *Astronomy and Astrophysics - A&A*, 2022, (in press). 10.1051/0004-6361/202142140 . insu-03479560v1

**HAL Id: insu-03479560**

**<https://insu.hal.science/insu-03479560v1>**

Submitted on 14 Dec 2021 (v1), last revised 21 Feb 2022 (v2)

**HAL** is a multi-disciplinary open access archive for the deposit and dissemination of scientific research documents, whether they are published or not. The documents may come from teaching and research institutions in France or abroad, or from public or private research centers.

L'archive ouverte pluridisciplinaire **HAL**, est destinée au dépôt et à la diffusion de documents scientifiques de niveau recherche, publiés ou non, émanant des établissements d'enseignement et de recherche français ou étrangers, des laboratoires publics ou privés.

# Near-infrared transmission spectrum of TRAPPIST-1 h using Hubble WFC3 G141 observations

A. Gressier<sup>1,2,3</sup>, M. Mori<sup>4</sup>, Q. Changeat<sup>5</sup>, B. Edwards<sup>5,6</sup>, J.P. Beaulieu<sup>2,7</sup>, E. Marcq<sup>1</sup>, and B. Charnay<sup>3</sup>

<sup>1</sup> LATMOS, CNRS, Sorbonne Université UVSQ, 11 boulevard d'Alembert, F-78280 Guyancourt, France e-mail: amelie.gressier@latmos.ipsl.fr

<sup>2</sup> Sorbonne Universités, UPMC Université Paris 6 et CNRS, UMR 7095, Institut d'Astrophysique de Paris, 98 bis bd Arago, 75014 Paris, France

<sup>3</sup> LESIA, Observatoire de Paris, Université PSL, CNRS, Sorbonne Université, Université de Paris, 5 place Jules Janssen, 92195 Meudon, France

<sup>4</sup> Department of Astronomy, University of Tokyo, Tokyo, Japan

<sup>5</sup> Department of Physics and Astronomy, University College London, London, United Kingdom

<sup>6</sup> AIM, CEA, CNRS, Université Paris-Saclay, Université de Paris, F-91191 Gif-sur-Yvette, France

<sup>7</sup> School of Physical Sciences, University of Tasmania, Private Bag 37 Hobart, Tasmania 7001 Australia

Received 3 September 2021/ Accepted 27 November 2021

## ABSTRACT

**Context.** The TRAPPIST-1 planetary system is favourable for transmission spectroscopy and offers the unique opportunity to study rocky planets with possibly non-primary envelopes. We present here the transmission spectrum of the seventh planet of the TRAPPIST-1 system, TRAPPIST-1 h ( $R_p=0.752 R_\oplus$ ,  $T_{eq}=173K$ ) using Hubble Space Telescope (HST), Wide Field Camera 3 Grism 141 (WFC3/G141) data.

**Aims.** Our purpose is to reduce the HST observations of the seventh planet of the TRAPPIST-1 system and, by testing a simple atmospheric hypothesis, to put a new constraint on the composition and the nature of the planet.

**Methods.** First we extracted and corrected the raw data to obtain a transmission spectrum in the near-infrared (NIR) band (1.1-1.7 $\mu m$ ). TRAPPIST-1 is a cold M-dwarf and its activity could affect the transmission spectrum. We corrected for stellar modulations using three different stellar contamination models; while some fit the data better, they are statistically not significant and the conclusion remains unchanged concerning the presence or lack thereof of an atmosphere. Finally, using a Bayesian atmospheric retrieval code, we put new constraints on the atmosphere composition of TRAPPIST-1h.

**Results.** According to the retrieval analysis, there is no evidence of molecular absorption in the NIR spectrum. This suggests the presence of a high cloud deck or a layer of photochemical hazes in either a primary atmosphere or a secondary atmosphere dominated by heavy species such as nitrogen. This result could even be the consequence of the lack of an atmosphere as the spectrum is better fitted using a flat line. Variations in the transit depth around 1.3 $\mu m$  are likely due to remaining scattering noise and the results do not improve while changing the spectral resolution. TRAPPIST-1 h has probably lost its atmosphere or possesses a layer of clouds and hazes blocking the NIR signal. We cannot yet distinguish between a primary cloudy or a secondary clear envelope using HST/WFC3 data; however, in most cases with more than  $3\sigma$  confidence, we can reject the hypothesis of a clear atmosphere dominated by hydrogen and helium. By testing the forced secondary atmospheric scenario, we find that a CO-rich atmosphere (i.e. with a volume mixing ratio of 0.2) is one of the best fits to the spectrum with a Bayes factor of 1.01, corresponding to a  $2.1\sigma$  detection.

**Key words.** Planets and satellites: atmospheres — Techniques: photometric, Techniques: spectroscopic

## 1. Introduction

The TRAPPIST-1 planetary system was discovered by Gillon et al. (2016) and Gillon et al. (2017), using the Transiting Planets and PlanetIsimals Small Telescope (Gillon et al. 2011, 2013). TRAPPIST-1 h is the most outer planets detected in this system, its detection was first suggested in Gillon et al. (2017), but later confirmed in Luger et al. (2017b). Further observations using Spitzer and K2 photometry followed the discovery to better constrain planetary parameters (Delrez et al. 2018; Ducrot et al. 2018; Burdanov et al. 2019; Ducrot et al. 2020). Since then, important scientific efforts have been carried out to observe, characterise, and model the seven planets orbiting this M8-type star. This is motivated by the fact that the TRAPPIST-1 system offers the most favourable conditions to study rocky planets in the hab-

itable zone, that is to say planets that could harbour liquid water on their surface as defined in Kasting et al. (1993).

TRAPPIST-1 is close (39.14 light years), cool (2559 K), and small ( $0.117 R_\odot$ ), making it favourable for observations (Gillon et al. 2017). On the other hand, the star is also the limiting factor in studying the atmosphere of TRAPPIST-1 planets. M-type stars stay for millions of years in the pre-main sequence (PMS) phase, during which planets are exposed to strong non-thermal extreme UV (EUV) and far-UV irradiation, which is expected to lead to atmospheric hydrodynamical escape (Vidal-Madjar et al. 2003; Bourrier et al. 2017b) and a runaway greenhouse effect (Ramirez & Kaltenegger 2014). TRAPPIST-1 is a very cold M-dwarf, but it is supposedly very active with strong flaring events (Vida et al. 2017) and EUV flux (Wheatley et al. 2017). Atmospheric erosion might have stripped all planets in the TRAPPIST-1 system of their atmospheres (Lammer et al.

**Table 1.** Stellar and planetary parameters used in this work

Parameter	Value
Spectral type	M8-V
$R_s$ ( $R_\odot$ )	$0.1170 \pm 0.0036$
$M_s$ ( $M_\odot$ )	$0.0802 \pm 0.0073$
$T_s$ (K)	$2559 \pm 50$
$\log(g)$	5.21
Fe/H	$0.040 \pm 0.080$
$R_p$ ( $R_\oplus$ )	$0.752 \pm 0.032$
$M_p$ ( $M_\oplus$ )	$0.331^{+0.056}_{-0.049}$
$a$ (AU)	$0.059 \pm 0.004$
$T_{\text{eff}}$ (K)	$173 \pm 4$
$S$ ( $S_\oplus$ )	$0.165 \pm 0.025$
$a/R_s$	$109 \pm 4$
$i$ (deg)	$89.76^{+0.05}_{-0.03}$
$e^a$	0
$b$	0.45
$P_{\text{orb}}$ (days)	$18.767^{+0.004}_{-0.003}$
$T_{\text{mid}}$ (BJD <sub>TDB</sub> )	$2\,458\,751.06983 \pm 0.00021^b$

**Notes.** Values are from Gillon et al. (2017) and Luger et al. (2017a).

<sup>(a)</sup> Fixed to zero <sup>(b)</sup> Obtained in this work

2003; Bolmont et al. 2017). Whether or not an atmosphere was sustained depends on the initial amount of accreted volatiles during the planetary formation phase, and the intensity of the atmospheric escape due to the star activity.

The TRAPPIST-1 planetary system is very compact, all the planets are within 0.06 AU and they are co-planar (Luger et al. 2017a,b; Delrez et al. 2018). In addition to this, they all have a circularised orbit with eccentricities below 0.01 (Gillon et al. 2017; Luger et al. 2017b) and present gravitational interactions forming a resonant chain, thus suggesting that the system had a relatively peaceful history. TRAPPIST-1 h is the furthest and the smallest known planet of this planetary system. It has a radius of  $0.752 \pm 0.032 R_\oplus$  and a mass of  $0.331^{+0.056}_{-0.049} M_\oplus$  (Luger et al. 2017b; Gillon et al. 2017), which suggests a density similar to that of Mars ( $\sim 4000 \text{ kg/m}^3$ ). The planetary parameters are detailed in Table 1 along with stellar and orbital parameters of the system.

Two possible formation scenarios have been proposed for the TRAPPIST-1 system and in particular for TRAPPIST-1 h. The first one suggests that all the planets that formed beyond the water frost line migrated inwards, causing the resonance, and they are now located between planets g and h. This possibility was proposed in the discovery papers Gillon et al. (2017) and Luger et al. (2017b), but also detailed in Ormel et al. (2017), Tamayo et al. (2017), and Coleman et al. (2019). If TRAPPIST-1 h formed far from the host star, it could be volatiles-rich because the atmospheric escape would only remove between 1 and 10% of the total planet mass (Tian & Ida 2015; Bolmont et al. 2017; Bourrier et al. 2017b; Turbet et al. 2020a). TRAPPIST-1 h could also have formed in situ, and a short migration or an eccentricity damping could have caused the resonant chain (MacDonald & Dawson 2018). In this case, the planet is probably dry (Turbet et al. 2020a) because of the strong atmospheric erosion.

On the other hand, TRAPPIST-1 h, being the furthest planet of the system, might have had a more important quantity of initial gas than inner planets. It could have formed with TRAPPIST-1 f and g in a different part of the proto-planetary disk leading to a different bulk composition (Papaloizou et al. 2018; Turbet et al. 2020a). Volatiles could also have been brought after by cometary

impacts or degassing (Kral et al. 2018; Dencs & Regály 2019; Turbet et al. 2020a; Kimura & Ikoma 2020), and this is favoured for outer planets because volatiles' impacts dominate over the impact erosion mechanism (Kral et al. 2018).

For close-in planetary systems, the effects of gravitational tides by the star on the planets are important and shape the orbital dynamics, that is to say they slow down the rotation rate, reduce the obliquity, and circularise the orbit. As shown in Turbet et al. (2018), the evolution timescales for TRAPPIST-1 h is 7 million years for the rotation and 80 million years for the obliquity. Knowing the age of the TRAPPIST-1 system, which is 8 billion years (Burgasser & Mamajek 2017), it is likely that TRAPPIST-1 h is in a synchronous rotation state. However, tidal heating is unlikely to be the dominant interior heating process for outer planets (Turbet et al. 2018; Makarov et al. 2018; Dobos et al. 2019) as compared with direct atmospheric warming. The received stellar flux is indeed two orders of magnitude higher than the tidal heating for TRAPPIST-1 h (Turbet et al. 2020a). It is then unlikely that TRAPPIST-1 h tidal heating caused the melting of the mantle leading to the out-gassing of volcanic gases (Turbet et al. 2020a).

As of today, TRAPPIST-1 h is the only planet of the system for which the near-infrared (NIR) spectrum (1.1-1.7  $\mu\text{m}$ ) from the Hubble Space Telescope (HST) Wide Field Camera 3 Grism 141 (WFC3/G141) has not been published. The other planets' spectra have already been studied with different pipelines and stellar contamination models in de Wit et al. (2016) and de Wit et al. (2018), Zhang et al. (2018), and Wakeford et al. (2019). From these analyses, we learned that the TRAPPIST-1 planets probably do not have an  $\text{H}_2$ , He extended atmosphere. However, it was impossible to rule out this hypothesis using only HST/WFC3 (de Wit et al. 2018; Moran et al. 2018). All spectra are consistent with flat spectra and could be fitted with different models including a high altitude cloud cover and/or a high metallicity hydrogen-rich atmosphere. A featureless spectrum could also be the result of the absence of an atmosphere around these planets. However, Bourrier et al. (2017b) and Bourrier et al. (2017a) analysed Lyman- $\alpha$  HST/STIS transits of TRAPPIST-1 b and c and detected a decrease in the flux, which might hint at the presence of an extended hydrogen exosphere.

We present the first attempt to characterise the atmosphere of the seventh planet of the system, TRAPPIST-1 h. In Sec. 2.1, we analyse the HST/WFC3 G141 raw data using the python package Iraclis (Tsiaras et al. 2016b,a, 2018) and detail the stellar contamination models used to correct our spectrum in Sec. 2.2. Section 2.3 presents the atmospheric characterisation of TRAPPIST-1 h. First, different atmospheric scenarios are discussed based on the recent review by Turbet et al. (2020a). Then, we detail the atmospheric retrieval set-ups we performed using the Bayesian radiative transfer code TauREx3 (Al-Refaie et al. 2021)<sup>1</sup>. Finally, we discuss our findings in Sec. 4.

## 2. Data analysis

### 2.1. Hubble WFC3 data reduction and extraction

We used the raw spatially scanned spectroscopic images obtained from Proposal 15 304 (PI: Julien de Wit) in the Mikulski Archive for Space Telescope<sup>2</sup>. Three transit observations of TRAPPIST-1 h were acquired using the Grism 256 aperture and 256 x 256 sub-array with an exposure time of 112.08 s. We refer

<sup>1</sup> [https://github.com/ucl-exoplanets/TauREx3\\_public](https://github.com/ucl-exoplanets/TauREx3_public)

<sup>2</sup> <https://archive.stsci.edu/hst/>

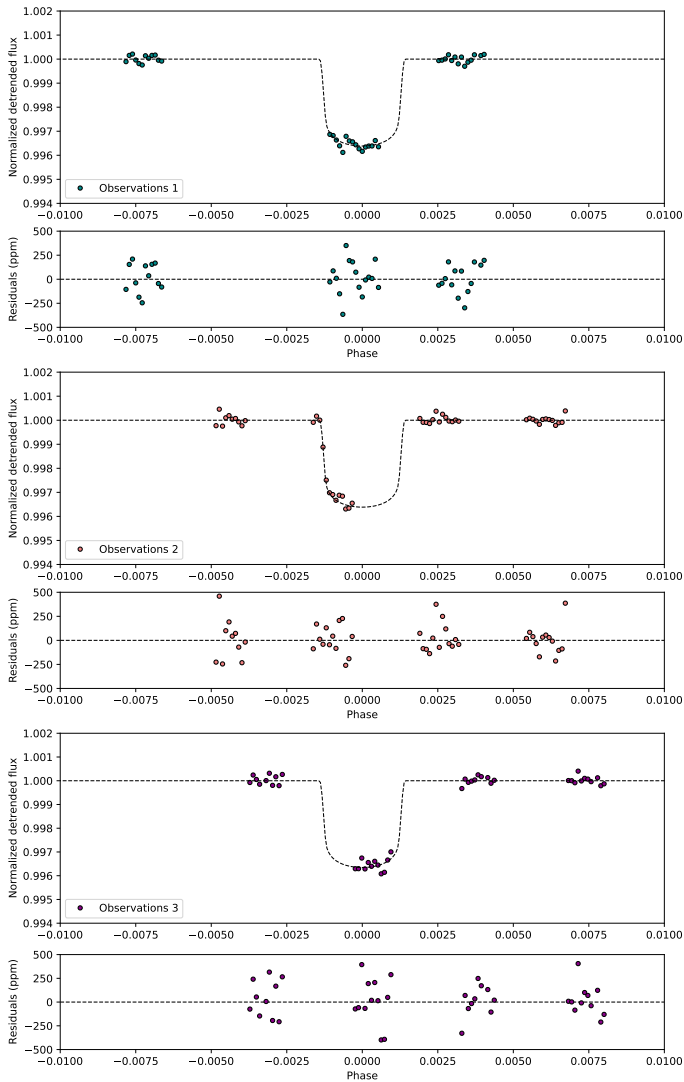


**Fig. 1.** White light curve fits for the three visits on TRAPPIST-1h (top: July 2017, middle: September 2019, and bottom: July 2020). For every observation, we show the de-trended flux (colour points) and the best fit model (dotted lines) along with the residuals from the best fit model.

to the data taken in July 2017, September 2019, and July 2020 as Observations 1, 2, and 3, respectively. Each visit is made up of four HST orbits, with 60 exposures in Observation 2 and 50 exposures for Observations 1 and 3, each being made in the forward spatial scan mode.

To reduce and analyse the data, we used Iraclis<sup>3</sup> (Tsirias et al. 2016b,a, 2018), a publicly available pipeline, dedicated to the analysis of the scanned spectroscopic observations obtained with the near-infrared grisms (G102, G141) of Hubble’s Wide Field Camera 3. The reduction of the raw observations follows these steps: zero-read subtraction, reference pixels correction, non-linearity correction, dark current subtraction, gain conversion, sky background subtraction, flat-field correction, and corrections for bad pixels and cosmic rays. For all three observations, we used the reduced spatially scanned spectroscopic images to extract the white and spectral light curves. We used the default ‘low’ resolution from Iraclis for the spectral light curves bins, which correspond to a resolving power of around 50 at 1.4  $\mu\text{m}$ .

Using the extracted light curves and the time of the observations, we first looked for contamination from others TRAPPIST-1 planets transits using the python package PyLightcurve (Tsirias et al. 2016a)<sup>4</sup>. The planets and transit parameters were set to those of Gillon et al. (2017). TRAPPIST-1 c was also transiting during the second orbit of the first observation (July 2017) and we then suppressed this orbit from the rest of the analysis. We plot in the appendix B.1 the extracted raw flux and the corresponding predicted transits of TRAPPIST-1 planets for the three visits.

The first orbit always presents a stronger wavelength-dependent ramp than the other orbits and is usually suppressed from the analysis. However, we decided to keep the first HST orbit in every transit observation in order to conserve an out-of-transit baseline and correctly fit the transit parameters. Indeed, every attempt was made to keep as many exposures as possible. For Observations 1 and 2, we removed the first two exposures of these first orbits, but kept all exposures of every subsequent orbit. However, for Observation 3, an adequate fit could only be obtained by removing the first exposure of every orbit, a practice which is normal as these exposures present significantly lower counts than the following exposures (e.g. Deming et al. 2013; Tsirias et al. 2016b; Edwards et al. 2021).

We fitted the white light curves and the spectral light curves using the transit model from PyLightcurve (Tsirias et al. 2016a) and the Markov chain Monte Carlo (MCMC) method implemented in emcee (Foreman-Mackey et al. 2013). For the white light curve fitting of all the observations, the only free planetary parameters are the mid-transit time and the planet-to-star radius ratio. The other planetary parameters were fixed to the values from Luger et al. (2017a) ( $a/R_s = 109 \pm 4$  and  $i = 89.76^\circ$ ) and stellar parameters are from Gillon et al. (2017) ( $T_s = 2559 \pm 50$  K,  $\log(g) = 5.21$ ,  $\text{Fe}/\text{H} = 0.04$ ). We also fitted for the coefficients  $ra$ ,  $rb_1$ , and  $rb_2$ . We adopted the parameterisation of Claret et al. (2012) and Claret et al. (2013) with four parameters to describe the limb-darkening coefficient. We used the PHOENIX database (Claret 2018) and ExoTETHyS package (Morello et al. 2020) to obtain the limb-darkening coefficients for the white light curve analysis but also in every wavelength bin for the spectral curves fitting (see Table 2). We accounted for the ramp time-dependent systematic effect in the white light curve fitting using the following formula with  $t$  being the time,  $t_0$  the beginning time of each HST orbit,  $T_0$  the mid-transit time,  $n_{\text{scan}}$  a normalisation factor,  $ra$  the slope of a linear systematic trend, and  $(rb_1, rb_2)$  the coefficients of the exponential systematic trend along each HST orbit:

$$R_w(t) = n_w^{\text{scan}}(t)(1 - r_a(t - T_0))(1 - r_{b_1}e^{r_{b_2}(t - t_0)}). \quad (1)$$

We then fitted for the planet-to-star radius ratio in every wavelength band. We used the white light curve divide method (Kreidberg et al. 2014) along with a spectral-dependent visit-long slope (Tsirias et al. 2018) model to account for the systematic effects as follows, with  $\chi_\lambda$  being the slope for the wavelength-dependent systematic effects along each orbit,  $LC_w$  the white light curve signal, and  $M_w$  the white light curve best fit model:

$$R_\lambda(t) = n_\lambda^{\text{scan}}(t)(1 - \chi_\lambda(t - T_0))\frac{LC_w}{M_w}. \quad (2)$$

The white light curve fits for the three different observations are shown in Fig. 1. The planet-to-star radius ratio are found to be compatible with  $0.0575 \pm 0.0006$  for Observation 1,  $0.0565 \pm 0.0009$  for Observation 2, and  $0.0575 \pm 0.0012$

<sup>3</sup> <https://github.com/ucl-exoplanets/Iraclis>

<sup>4</sup> <https://github.com/ucl-exoplanets/pylightcurve>



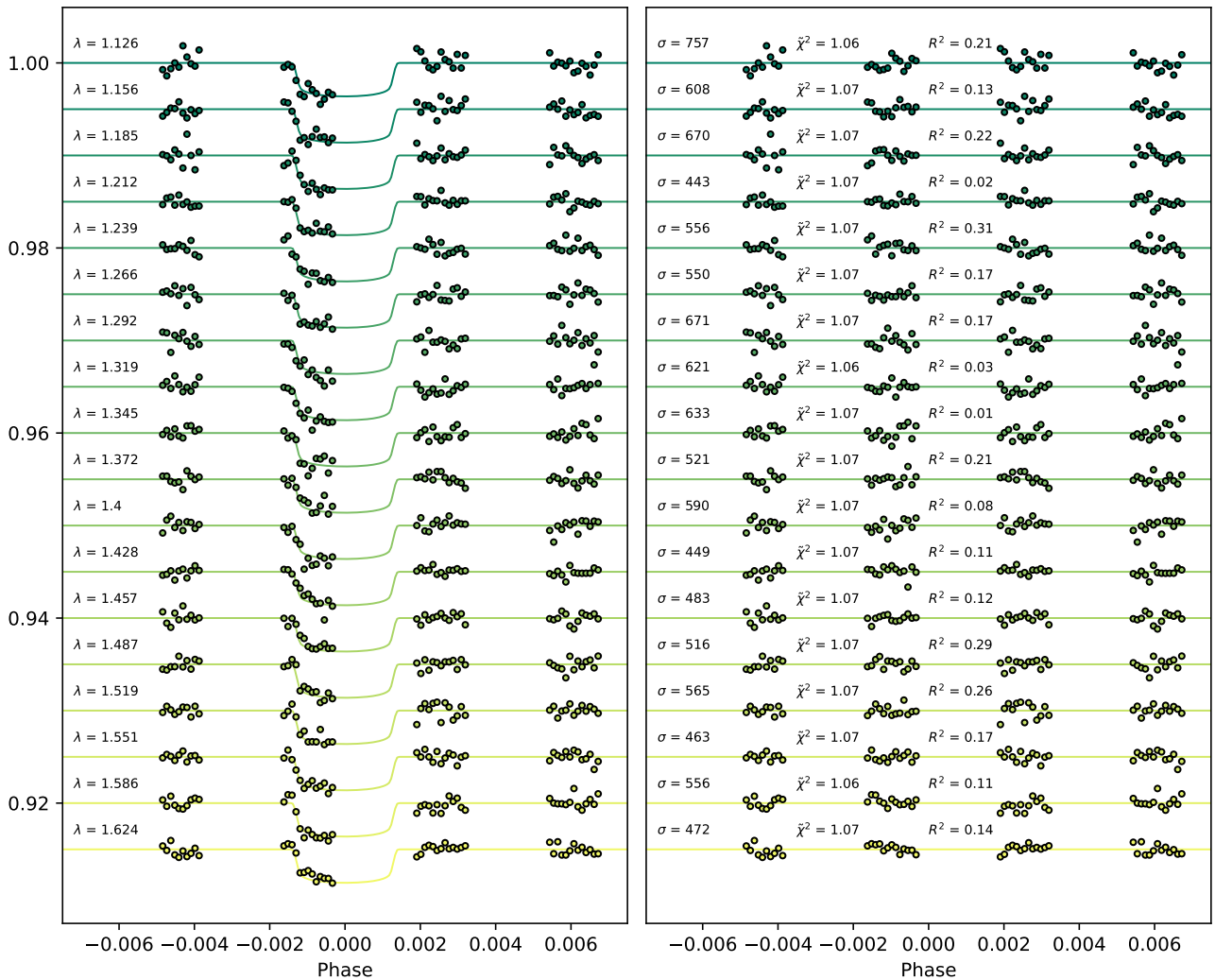


**Fig. 2.** Spectral light curve fits of the September 2019 visit (Observation 2) for the transmission spectra of TRAPPIST-1 h. An artificial offset in the y-axis was applied for clarity. For each light curve, the left panel shows the de-trended spectral light curves with the best fit model in dotted lines with the centred wavelength and the right panel shows the residuals and values for the standard deviation ( $\sigma$ ) in ppm, the reduced Chi-squared ( $\chi^2$ ), and the auto-correlation ( $R^2$ ).

for Observation 3. We found the following mid-transit times in  $\text{BJD}_{\text{TDB}}$ :  $2\,458\,319.4282 \pm 0.00020$  for Observation 1,  $2\,458\,751.06983 \pm 0.00021$  for Observation 2, and  $2\,459\,051.3428 \pm 0.00021$  for Observation 3. The spectral light curve fit for the second observation is presented in Fig. 2, while the two other spectral light curve fits are in appendix B.2. We computed the final transmission spectrum by combining the three spectral fits using a weighted mean of the transmission spectra. After the initial white light curve fit, the errors on each exposure were scaled to match the root mean square of the residuals. The white fitting was then performed a second time with these scaled errors. A similar scaling was also applied to the spectral light curves. This method ensures that the recovered uncertainties on the transit depth are not underestimated (Tsiaras et al. 2016b). The transmission spectra and the recovered final transit depth are overplotted in Fig. 3, along with the corresponding residuals. We note a rise in the transit depth around  $1.3\,\mu\text{m}$ . All three observations exhibit similar features over these regions, suggesting this is of astrophysical origin and part of the transit spectrum and not a contamination, or poor fitting, of a single visit. We also present in appendix B.3 the three white light curve fits in the same plot using a planet-to-star radius ratio weighted

by the mean of the three white light curve best fits for the transit model. The combined extracted spectrum and the uncertainties are presented in Table 2.

## 2.2. Modelling the stellar contamination

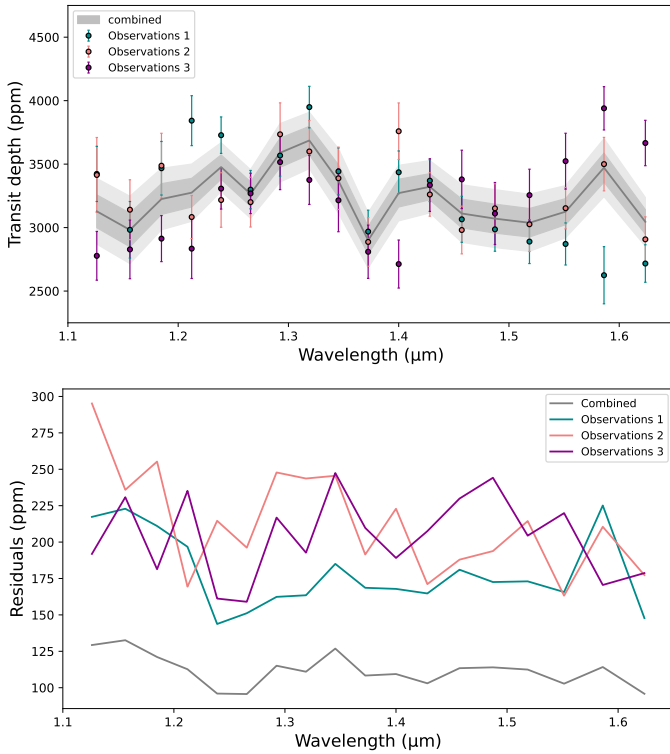
TRAPPIST-1 is known for presenting a heterogeneous photosphere that can lead to a misinterpretation of the transmission spectra. The goal of this section is to use different existing models to correct our spectrum for a stellar contribution. The star presents a  $\sim 1\%$  photometric variability in the I+z bandpass interpreted as active regions rotating in and out of view (Gillon et al. 2016). Rackham et al. (2018) show that it would cause a non-negligible effect (transit light source effect, TLSE) on the transmission spectrum if the variability is consistent with rotational modulations. Several previous studies have examined the stellar surface models using a variety of methods, but their results are not consistent. In the present study, three stellar models from three studies, Zhang et al. (2018), Morris et al. (2018), and Wakeford et al. (2019), were introduced and examined.

Table 3 shows the temperature and the covering fraction of each component for each model. We note that  $T_i$  is the tempera-

**Table 2.** Combined transit depth, associated uncertainties and limb-darkening coefficients.

Wavelength ( $\mu\text{m}$ )	Bandwidth ( $\mu\text{m}$ )	Transit depth (ppm)	Error (ppm)	Limb-darkening coefficients			
				a1	a2	a3	a4
1.1262	0.0308	3128.22	129.30	2.0139	-1.6261	0.8709	-2.0398
1.1563	0.0293	2981.61	132.61	2.1956	-2.0725	1.2403	-0.3147
1.1849	0.0279	3224.87	121.09	2.1292	-1.9036	1.0964	-0.2708
1.2123	0.0269	3275.06	112.69	1.9514	-1.5303	0.8020	-0.1849
1.2390	0.0265	3476.20	95.97	1.9236	-1.5957	0.8838	-0.2137
1.2657	0.0269	3264.82	95.65	2.0255	-1.8405	1.0765	-0.2698
1.2925	0.0267	3589.24	115.10	2.1105	-2.1495	1.3561	-0.3578
1.3190	0.0263	3686.39	110.98	2.1650	-2.2486	1.4262	-0.3772
1.3454	0.0265	3368.20	126.87	1.2204	-0.1088	-0.1857	0.0789
1.3723	0.0274	2900.07	108.34	1.0023	0.4493	-0.6644	0.2195
1.4000	0.0280	3271.69	109.38	0.9553	0.4582	-0.6187	0.1988
1.4283	0.0285	3321.59	103.01	0.7774	0.7086	-0.7252	0.2128
1.4572	0.0294	3111.09	113.41	0.9247	0.4694	-0.6071	0.1921
1.4873	0.0308	3070.67	113.98	1.0279	0.2998	-0.530181	0.18063
1.5186	0.0318	3037.95	112.45	1.2541	-0.1103	-0.2727	0.1188
1.5514	0.0337	3125.30	102.78	1.5025	-0.6408	0.1247	0.0082
1.5862	0.0360	3472.00	114.20	1.7942	-1.3368	0.6809	-0.1553
1.6237	0.0390	3045.52	95.82	1.9296	-1.7566	1.0358	-0.2629
1.3750	0.5500	3268.70	51.38	2.009	-1.7704	1.0225	-0.2546

**Notes.** The final transmission spectrum was computed in ppm using the three HST/WFC3 G141 transit observations from July 2017, September 2019, and July 2020 on TRAPPIST-1 h.



**Fig. 3.** Recovered transit depths for the three observations and combined transmission spectrum with 1 and 2 $\sigma$  uncertainty ranges (top). First, we suppressed the white light curve values from each visit raw flux, then, we computed the weighted mean, and finally we added the mean white light curve value to obtain the transit depth. Residuals are from the spectral light curves analysis and the combined spectrum (bottom).

ture,  $f_i$  is the covering fraction at the photosphere, and  $f'_i$  is the covering fraction at the transit chord. The M18 model is the best

fit model from Morris et al. (2018). Z18 is the best fit contamination model taken from Table 16 in Zhang et al. (2018). W19 is the  $3T_{c+m}$  model from Wakeford et al. (2019). We note that what we call the W19 model here is not the best fit model in their analysis, as they conclude that TLSE is not significant in their data, but they did not exclude  $3T_{c+m}$ .

**Table 3.** Summary of the adopted TRAPPIST-1 stellar models.

Model	Z18	M18	W19
$T_1(\text{K})$	2000	2500	2400
$T_2(\text{K})$	2400	5300	3000
$T_3(\text{K})$	3000	–	5800
$f_1$	0.38	0.999952	0.64
$f_2$	0.14	$4.8 \times 10^{-5}$	0.35
$f'_1$	0.10	1.0	0.646
$f'_2$	0.45	0.0	0.354

We define the wavelength-dependent contamination factor  $\epsilon_\lambda$  as

$$\delta_\lambda = \epsilon_\lambda \times \delta_{\text{real},\lambda}, \quad (3)$$

where  $\delta_\lambda$  is the measured transit depth and  $\delta_{\text{real},\lambda}$  is the actual transit depth. For each stellar surface model,  $\epsilon_\lambda$  was calculated as

$$\epsilon_\lambda = \frac{f'_1 S_{1,\lambda} + f'_2 S_{2,\lambda} + f'_3 S_{3,\lambda}}{f_1 S_{1,\lambda} + f_2 S_{2,\lambda} + f_3 S_{3,\lambda}} \quad (4)$$

$$f_3 = 1 - f_1 - f_2 \quad (5)$$

$$f'_3 = 1 - f'_1 - f'_2, \quad (6)$$

where  $S_{i,\lambda}$  is the stellar flux of each temperature component. We used the BT-Settl model for each temperature, with the metallicity  $[\text{Fe}/\text{H}] = 0$  dex and the stellar surface gravity  $\log g$  at 5.2, from the SVO theoretical spectra web server (<sup>5</sup>).

<sup>5</sup> <http://svo2.cab.inta-csic.es/theory/newov2/>

## 2.3. Atmospheric modelling

### 2.3.1. Possible atmospheric scenarios

Turbet et al. (2020a) reviewed the different atmospheric scenarios for TRAPPIST-1 planets. We discuss the different possibilities mentioned for TRAPPIST-1 h, such as a  $\text{H}_2/\text{He}$  rich atmosphere, a  $\text{H}_2\text{O}$  envelope, as well as a  $\text{O}_2$ , a  $\text{CO}_2$ , a  $\text{CH}_4/\text{NH}_3$ , or a  $\text{N}_2$  dominated atmosphere. First, numerical modelling using mass and radius measurements have shown that a  $\text{H}_2/\text{He}$  envelope is unlikely for all TRAPPIST-1 planets. Turbet et al. (2020a) constructed a mass-radius relation using the Grimm et al. (2018) atmospheric climate calculation and estimated that for a ‘cold’ scenario assuming 100 x solar metallicity and based on TRAPPIST-1 h irradiation, the maximum hydrogen to core mass fraction is  $4 \times 10^{-4}$  for a clear atmosphere. Using the estimation of Wheatley et al. (2017) for the EUV flux received by the planet ( $10^2 \text{ erg.s}^{-1}.\text{cm}^{-2}$ ) and the results from Bolmont et al. (2017), Bourrier et al. (2017b) and Bourrier et al. (2017a), they computed the equivalent mass loss over the age of the system (8 billion years) and found  $10^{22} \text{ kg}$  (i.e.  $5 \times 10^{-3}$  mass fraction). A hydrogen-rich envelope could be ripped out in  $\sim 100$  million years for TRAPPIST-1 h (Turbet et al. 2020a), meaning that this type of atmosphere is not completely impossible but unstable and unlikely to be sustained around this low mass planet. The recent publication by Hori & Ogihara (2020) has also shown that the total mass loss over the planet lifetime is supposedly higher than the initial amount of accreted gas.

Regarding a water-rich atmosphere scenario, Turbet et al. (2019a), Turbet et al. (2020b) and Turbet et al. (2020a) estimated the water content in TRAPPIST-1 planets by taking the runaway greenhouse limit into account, while Bourrier et al. (2017b) investigated the hydrodynamic water loss. Combining those two pieces of information leads to the conclusion that TRAPPIST-1 h could have lost less than three Earth oceans and could have retained water in its atmosphere or surface. Lincowski et al. (2019) show that  $\text{O}_2$  atmospheres would be the best candidate for TRAPPIST-1 planets as a remnant of  $\text{H}_2\text{O}$  erosion and Wordsworth et al. (2018) determine that  $\text{O}_2$  build-up is limited to one bar for TRAPPIST-1h.

We note that  $\text{NH}_3$  and  $\text{CH}_4$  are highly sensitive to photo-dissociation (Turbet et al. 2018) and for TRAPPIST-1h to sustain a  $\text{CH}_4$  or a  $\text{NH}_3$  rich atmosphere would require an important source of those species. Assuming an Earth-like methane production rate, the planet could have a concentration up to 0.3% (Rugheimer et al. 2015). However, methane or ammonia photolysis rates could decrease via the formation of high altitude clouds or hazes (Sagan & Chyba 1997; Wolf & Toon 2010; Arney et al. 2016).

An Earth-like atmosphere, that is one bar and a  $\text{N}_2$  rich atmosphere, might be stable against stellar wind for TRAPPIST-1 h if  $\text{CO}_2$  is abundant (Dong et al. 2018, 2019);  $\text{CO}_2$  could accumulate in TRAPPIST-1 planets (Lincowski et al. 2019) because it is less sensitive to atmospheric escape (Dong et al. 2017, 2018, 2019). However, Turbet et al. (2018) and Turbet et al. (2020a) show that TRAPPIST-1 h would probably experience a  $\text{CO}_2$  collapse. The planet is far from the star and probably tidally locked, favouring  $\text{CO}_2$  surface condensation. Furthermore,  $\text{CO}$  and  $\text{O}_2$  could also be found in the case of a  $\text{CO}_2$  rich atmosphere due to the photo-dissociation of  $\text{CO}_2$  and the low recombination of  $\text{CO}$  and  $\text{O}_2$  (Gao et al. 2015; Hu et al. 2020).

Finally, a water ocean at the surface of TRAPPIST-1 h, implying a potential habitability, is unlikely. As the planet is beyond the  $\text{CO}_2$  collapse region, the atmosphere does not warm the surface (Turbet et al. 2020a). To counterbalance the  $\text{CO}_2$  con-

densation, the planet would require a very thick  $\text{CO}_2$  atmosphere with volcanic gases such as  $\text{H}_2$  and  $\text{CH}_4$ , but, as explained above, neither  $\text{H}_2$  nor  $\text{CH}_4$  are expected to be stable in the TRAPPIST-1 h atmosphere (Pierrehumbert & Gaidos 2011; Wordsworth et al. 2017; Ramirez & Kaltenegger 2017; Lincowski et al. 2018; Turbet et al. 2018, 2019b, 2020b). Very few observational constraints have been brought on TRAPPIST-1 planets, leaving a wide range of atmospheric possibilities. The goal of the following section is to analyse the TRAPPIST-1 h IR spectrum with regards to the predictions mentioned above in order to bring new constraints and prepare further observations.

### 2.3.2. Retrieval analysis set-up

We used TauREx3 (Al-Refaie et al. 2021; Al-Refaie et al. 2021) and the nested sampling algorithm Multinest (Feroz et al. 2009) with an evidence tolerance of 0.5 and 1500 live points to perform the atmospheric retrieval analysis. TauREx3 is a fully Bayesian code that maps the atmospheric parameters space to find the best fit model for the transmission spectrum. It includes the molecular line lists from the ExoMol project (Tennyson et al. 2016; Chubb et al. 2021), HITEMP (Tennyson & Yurchenko 2018), and HITRAN (Rothman et al. 1987; Rothman et al. 2013). We simulated the atmosphere assuming a constant temperature-pressure profile and every layer of the simulated atmosphere is uniformly distributed in log spaced, with a total of 100 ranging from  $10^{-2}$  to  $10^5 \text{ Pa}$ . We included the collision-induced absorption (CIA) of  $\text{H}_2\text{-H}_2$  (Abel et al. 2011; Fletcher et al. 2018),  $\text{H}_2\text{-He}$  (Abel et al. 2012), and Rayleigh scattering. We used a wide range of temperatures (50-1000K) to adjust the temperature of the planet, using the effective temperature ( $\sim 173 \text{ K}$ ) as the initial value. The planetary radius was also fitted as a free parameter in the model and its value ranges from  $\pm 50\%$  of the published value reported in Table 1. The planetary radius fitted corresponds to the bottom of the atmosphere, that is the radius of the planet assumed to be at one bar here. Clouds were included using a simple grey opacity model and the top clouds pressure varies from  $10^{-2}$  to  $10^5 \text{ Pa}$ . We considered the following opacity sources:  $\text{H}_2\text{O}$  (Polyansky et al. 2018),  $\text{CO}_2$  (Rothman et al. 2010),  $\text{NH}_3$  (Yurchenko et al. 2011), and  $\text{CO}$  (Yurchenko & Tennyson 2014).

We performed two different atmospheric retrievals by forcing a primary and then a secondary atmosphere. We modelled the TRAPPIST-1 h atmosphere using  $\text{H}_2$ ,  $\text{He}$ , and  $\text{N}_2$  as fill gas and  $\text{H}_2\text{O}$ ,  $\text{CO}$ ,  $\text{CO}_2$ ,  $\text{NH}_3$ , and  $\text{CH}_4$  as trace gases. We note that  $\text{H}_2$ ,  $\text{He}$ , and  $\text{N}_2$  do not display features in the spectrum; they contribute to the continuum and shape the mean molecular weight. The ratio between  $\text{H}_2$  and  $\text{He}$  abundances was fixed to the solar value of 0.17, while the ratio between the abundance of  $\text{N}_2$  over the abundance of  $\text{H}_2$  varied between  $10^{-12}$  and  $10^{-2}$  for the primary model and between  $10^{-12}$  and  $10^4$  for the secondary scenario. The mean molecular weight can then evolve towards higher values and we were able to test a Hydrogen rich and then a Nitrogen rich atmosphere. The abundance of the other molecular absorption sources were included in the fit as a volume mixing ratio, allowing us to vary between  $10^{-12}$  and  $10^{-2}$ .

A flat-line model, only including a cloud deck, was performed to assess the significance of the different scenarios compared to a baseline. A baseline is representative of the lack of an atmosphere (e.g. an atmosphere with no spectral features) or a flat spectrum that can only be fitted by a high altitude cloud deck. The significance was computed using a Bayes factor, that is the difference of logarithm evidence between the best fit model and the baseline model. The Bayesian evidence was computed using Bayes’ theorem for a set of  $\theta$  parameters in a model  $H$  for the

data  $D$  (Feroz et al. 2009)

$$P(\theta|D, H) = \frac{P(D|\theta, H)P(\theta|H)}{P(D|H)}, \quad (7)$$

where  $P(\theta|D, H) \equiv P(\theta)$  is the posterior probability distribution,  $P(D|\theta, H) \equiv L(\theta)$  is the likelihood,  $P(\theta|H) \equiv \pi(\theta)$  is the prior, and  $P(D|H) \equiv E$  is the Bayesian evidence. The nested sampling method estimates the Bayesian evidence of a given likelihood volume and the evidence can be expressed as follows:

$$E = \int L(\theta)\pi(\theta) d\theta. \quad (8)$$

To compare the two  $H_0$  and  $H_1$  models, in our case the flat-line model and the primary or secondary scenario, we can compute the respective posterior probabilities, given the observed data set  $D$ ,

$$\frac{P(H_1|D)}{P(H_0|D)} = \frac{P(D|H_1)P(H_1)}{P(D|H_0)P(H_0)} = \frac{E_1 P(H_1)}{E_0 P(H_0)}, \quad (9)$$

where  $P(H_1)/P(H_0)$  is the a priori probability ratio for the two models, which can often be set to unity (Feroz et al. 2009). We used the logarithm version of the model selection to compute the Bayes factor,  $\Delta\log(E)$  between the flat-line and the tested model. This factor is also called the atmospheric detectability index (ADI) in Tsiaras et al. (2018) and defined as a positive value. The significance ( $\sigma$ ) represents the strength of a detection and it was estimated using a Kass & Raftery (1995), Trotta (2008), and Benneke & Seager (2013) formalism. We used Table 2 in Trotta (2008) and Table 2 in Benneke & Seager (2013) to find the equivalence between the Bayes factor and the significance  $\sigma$  and evaluate the strength of a detection. A Bayes factor of 1 corresponds to a  $2.1\sigma$  detection and is considered weak, a Bayes factor greater than 3 ( $3\sigma$ ) is considered significant, and one superior to 11 ( $5\sigma$ ) is considered as a strong detection. For the rest of the paper, we define  $\Delta\log(E) = \log(E_{\text{Atmospheric Model}}) - \log(E_{\text{Flat line}})$ . The atmospheric model can be considered a better fit compared to the flat line if the  $\Delta\log(E)$  is superior to 3.

### 3. Results

#### 3.1. Atmospheric retrieval results

There is no evidence of molecular absorption in the recovered spectrum of TRAPPIST-1h from the two retrieval results. Both primary and secondary retrieval analyses have logarithm evidence (109.92 and 110.18, respectively) comparable to the one of the flat-line model, that is 110.55. This result favours the scenario of a planet with no atmosphere, that is the presence of a high cloud layer in a primary atmosphere or a secondary envelope. It is consistent with previous work on other TRAPPIST-1 planets (de Wit et al. 2018; Wakeford et al. 2019; Zhang et al. 2018). Figure 4 (top) shows the extracted spectrum with the best-fit atmospheric results: flat-line (red), primary (blue), and secondary model (purple). The flat-line and the secondary best fit models are similarly flat with a transit depth around 3220 ppm, while the primary models are found around 3274 ppm. This difference is due to the different radius and temperature estimations depending on the scale height and the weight of the atmosphere. We present the correlations among parameters for the primary and the secondary model in Fig. 5. We overplotted the two posterior distributions for a direct comparison, but the values are displayed for the secondary best-fit model. The primary model posterior distribution alone is presented in Appendix B.4.

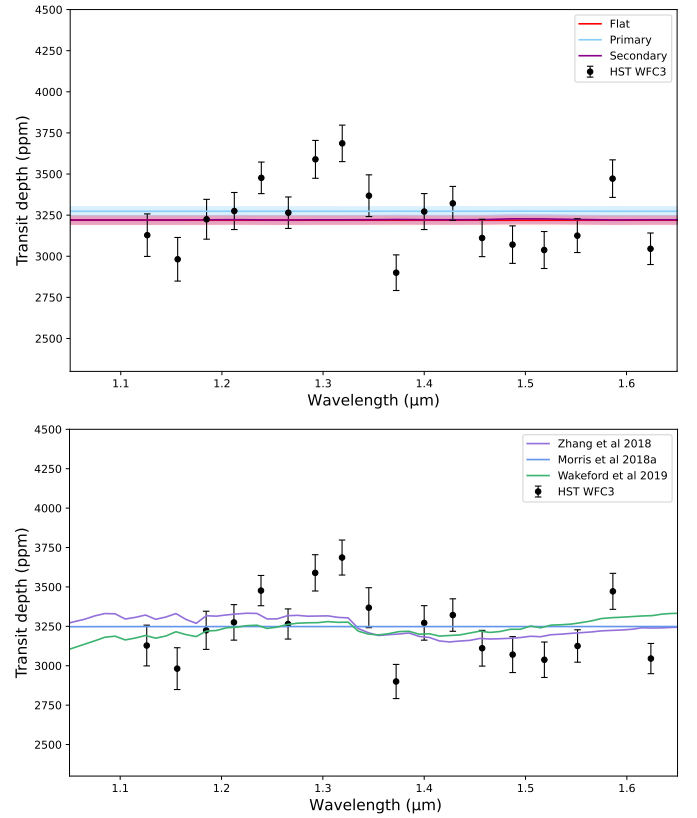


**Fig. 4.** Best-fit models to TRAPPIST-1 h HST WFC3 G141 data from atmosphere retrievals (top) and stellar contamination models based on Zhang et al. (2018), Wakeford et al. (2019), and Morris et al. (2018) (bottom).

The secondary atmospheric retrieval analysis estimates the radius to be  $0.69^{+0.03}_{-0.07} R_{\oplus}$  and the temperature reaches  $345^{+326}_{-196}$  K. The mean molecular weight distribution is bi-modal, and the code is able to retrieve two solutions: a light atmosphere with a 2.3 g/mol mean molecular weight and a heavier solution with a mean molecular weight reaching  $25.35^{+2.46}_{-23.02}$  g/mol corresponding to a 16 km scale height. This is correlated to the abundance of  $N_2$  retrieved as the ratio of inactive gases, that is  $\log(N_2/H_2)$ . When we allowed this ratio to increase beyond one, the best fit value was constrained to  $1.01^{+1.18}_{-6.13}$ . Yet, we note the presence of a second solution, around seven, which corresponds to the primary analysis retrieved value and creates the bi-modal distribution in the mean molecular weight. Nitrogen is the only parameter that impacts the value of the mean molecular weight as no constraints can be put on  $H_2O$ ,  $CH_4$ ,  $CO$ ,  $CO_2$ , and  $NH_3$ . From both posteriors distributions, we found the anti-correlation between the radius, temperature, and layer for top clouds, that is the radius decreases with increasing temperature and decreasing layer for top clouds. The latter is found really high in the atmosphere,  $\log(P_{\text{clouds}}) = 1.02^{+1.90}_{-1.72}$ , which corresponds to a cloud layer at approximately  $10^{-4}$  bar. Considering the pressure of this layer, it is likely that these clouds may not be condensation clouds, but rather photochemical mists or hazes with particles big enough not to have a spectral slope. From those two retrievals analyses, we show that the atmosphere must be either secondary (probably dominated by nitrogen) or primary with a very high photochemical haze layer. The two retrieval analyses have similar statistical results so we cannot favour one solution. We cannot rule out the hypothesis of a lack of an atmosphere either as the  $\log(E)$  of the

**Table 4.** Statistical results of the atmospheric retrieval analysis and the stellar contamination modelling on TRAPPIST-1h HST WFC3 G141 data.

Model	$\chi^2$	$\tilde{\chi}^2$	log(E)	$\Delta\log(E)$
Flat-line	64.95	3.61	110.55	N/A
Atmosphere primary	65.20	3.62	109.92	-0.63
Atmosphere secondary	65.25	3.62	110.18	-0.37
Stellar Zhang et al. (2018)	54.02	3.00	N/A	N/A
Stellar Wakeford et al. (2019)	60.70	3.37	N/A	N/A
Stellar Morris et al. (2018)	63.91	3.55	N/A	N/A
Corrected by Zhang et al. (2018)				
Flat-line	54.94	3.05	115.48	N/A
Atmosphere primary	50.54	2.81	115.02	-0.46
Atmosphere secondary	54.77	3.04	115.20	-0.28
Corrected by Wakeford et al. (2019)				
Flat-line	61.41	3.41	112.13	N/A
Atmosphere primary	61.91	3.44	111.51	-0.62
Atmosphere secondary	61.80	3.43	112.01	-0.12
Corrected by Morris et al. (2018)				
Flat-line	65.11	3.62	110.39	N/A
Atmosphere primary	65.28	3.63	109.79	-0.60
Atmosphere secondary	65.23	3.62	110.12	-0.27

**Notes.** Chi-squared ( $\chi^2$ ) and reduced chi-squared ( $\tilde{\chi}^2$ ) were computed using the result of the retrieval best-fit model and the stellar contamination models. Bayesian logarithm evidence (log(E)) and the Bayes factor ( $\Delta\log(E)$ ) were computed when applicable, i.e. only for the atmospheric retrieval analysis.

flat-line model remains the highest. We can reject a primary clear atmosphere as expected for this planet as the primary model does indeed require a layer of clouds to correctly fit the spectrum (see Sec. 4.1).

### 3.2. Including the stellar contamination

We present in Fig. 4 (bottom) the stellar contamination models and in Table 4 the statistical results on both the atmosphere and stellar models. We computed the chi-squared ( $\chi^2$ ) and the reduced chi-squared ( $\tilde{\chi}^2$ ) for all models and indicate the logarithm evidence (log(E)) from the retrieval analysis. The stellar contamination model of Zhang et al. (2018) is favoured, according to the chi-squared computation but none of the models we tested here are significant and can explain variations in the TRAPPIST-1h spectrum. In particular, the rise in the transit depth around  $1.3\mu\text{m}$  is not reproduced. To account for stellar contamination, we corrected our HST/WFC3 extracted spectrum by subtracting the stellar contributions using the Zhang et al. (2018), Wakeford et al. (2019), and Morris et al. (2018) formalism. We present in Table 5 the transit depth after subtraction of the stellar contamination for the three models and conduct the same retrieval analysis as in Sec. 3.1 on those corrected spectra. We overplotted all the different spectra as a comparison in appendix B.5. Statistical results on the retrieved corrected spectra are detailed in Table 4. For all the corrected spectra, the flat line is the favoured model, but the correction by Zhang et al. (2018) leads to the highest log(E). We present in Fig. 6 best-fit atmospheric retrieval results on the three spectra, while posterior distributions are in Appendix B.7, B.8, and B.9. We note transit depth variations at  $1.2\mu\text{m}$ ,  $1.45\mu\text{m}$ , and  $1.6\mu\text{m}$  on the primary best fit model on the spectrum corrected by Zhang et al. (2018). This is due to the contribution of  $\text{CO}_2$  to the best-fit solution, but the amount of  $\text{CO}_2$  is not constrained (see posterior distributions in Appendix B.7) and the model is not statistically significant. We also observe variations in the transit depth around  $1.5\mu\text{m}$  on the primary best fit model on the spectrum corrected by Morris

et al. (2018). This is due to the absorption of ammonia. Once again, this absorption is not constrained in terms of abundance and the log(E) remains below the one of the flat line. As an indication, we put the best-fit opacity contributions from those two models in appendix B.6. The correction made here to the spectra does improve the retrieval statistical results in the case of the Zhang et al. (2018) correction, but it does not lead to molecular detection and does not allow us to provide further constraints on the atmosphere of TRAPPIST-1 h.

To better constrain the stellar contamination, we also tried to add the optical value found in Luger et al. (2017a) using K2 photometry. As seen in the plot of Appendix B.10 and in the  $\chi^2$  computation results in Appendix A.2, the existing stellar models discussed here fit the spectrum poorly. First, we cannot ensure inter-instrument calibration at this accuracy and combining a different transit depth could lead to misinterpretations of the spectrum (Yip et al. 2020). In addition, it is possible that the stellar spot distribution has changed in the intervening time between the observations, but this is unlikely as they are not that far apart. K2 light curves were taken between 15 December 2016 and 4 March 2017, while the HST data were taken in July 2017, September 2019, and July 2020. A more likely explanation is that for both K2 and HST data, multiple transits were stacked, regardless of the phase of the star's rotation. If the stellar rotational phase and activity were different from time to time, the effect in the transmission spectrum would be suppressed when they are stacked. Adding this point does not further constrain the stellar contamination models in the case of TRAPPIST-1h.

## 4. Discussion

### 4.1. Primary clear atmosphere

We show in Sec. 3.1 that the HST/WFC3 extracted spectrum was compatible with either a secondary or a primary cloudy and hazy atmosphere if we retain the hypothesis of a presence of an atmosphere. In this section, we explore the case of a primary clear atmosphere by fixing the molecular absorption of the different



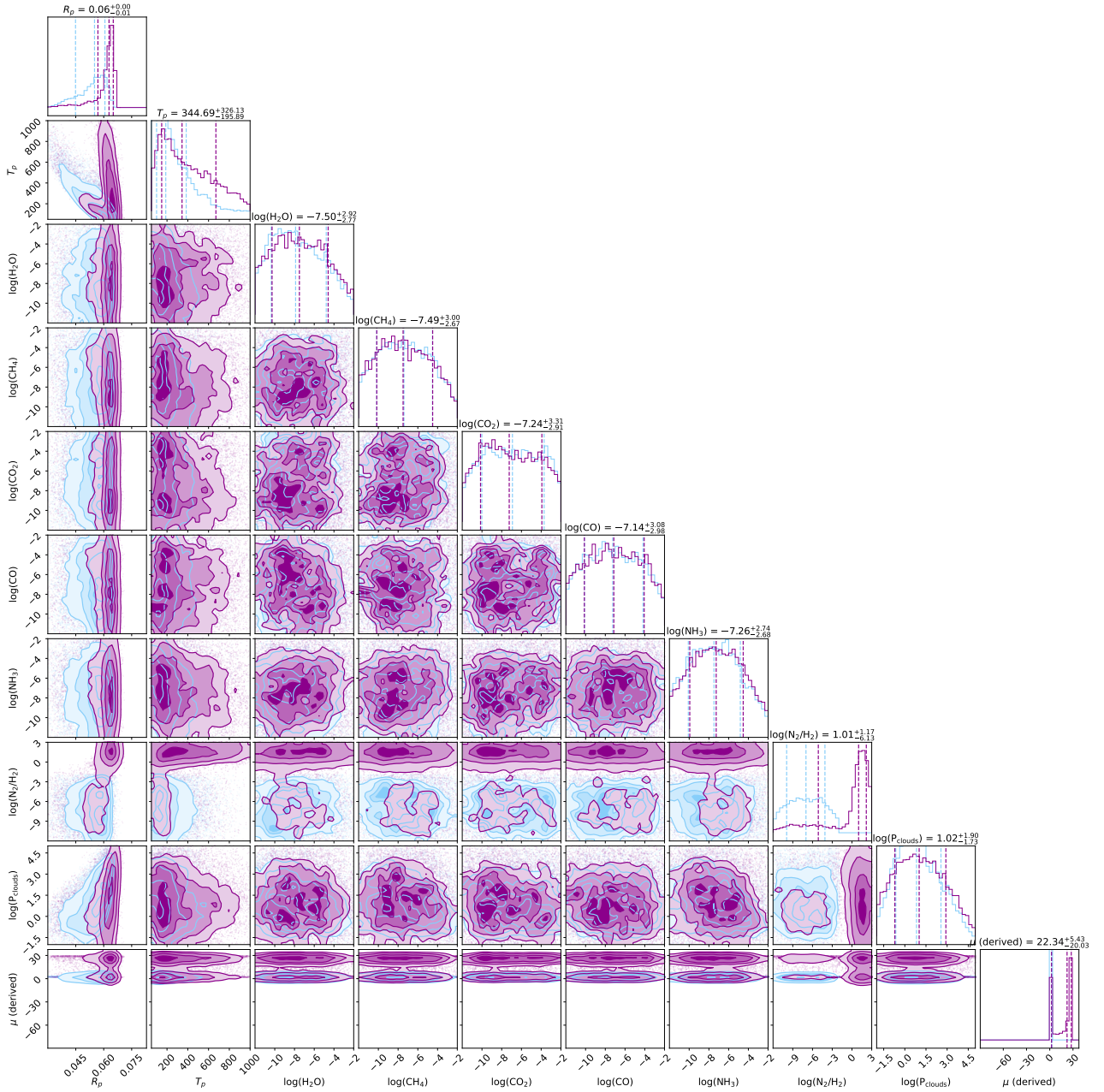


**Fig. 5.** Posterior distributions for the primary (blue) and the secondary retrieval (purple) on the extracted TRAPPIST-1h spectrum. Only the values from the secondary best-fit analysis are displayed.

species to  $10^{-3}$ , which forces spectral features. The temperature was allowed to vary between  $\pm 20\%$  of the equilibrium one (173K) and the radius was fitted between  $\pm 50\%$  of the published value. We tested six different opacity sources,  $\text{H}_2\text{O}$ ,  $\text{CO}_2$ ,  $\text{CO}$ ,  $\text{CH}_4$ ,  $\text{NH}_3$ , and  $\text{N}_2$ , separately by running a retrieval for each source. We included collision-induced absorption and Rayleigh scattering and fixed the  $\text{He}/\text{H}_2$  ratio to 0.17. The atmosphere was simulated as in Sec. 3.1, with 100 layers ranging between  $10^{-2}$  and  $10^5$  Pa.

We measured the size of a clear atmosphere in the case of TRAPPIST-1 h in those six configurations and show that a primary clear atmosphere is rejected in each case. We present in Table 6 best-fit results from the six tested scenarios. We indicate the radius, the temperature, and the mean molecular weight, and we estimate the corresponding scale height. For comparison, we also indicate the results from the flat-line model of Sec. 3.1.

Statistical results, that is to say the logarithm evidence, from primary clear models are below the one of the flat line, with an absolute difference of 3 or more, while including  $\text{H}_2\text{O}$ ,  $\text{CH}_4$ ,  $\text{NH}_3$ , or  $\text{N}_2$ . This result indicates that a primary clear atmosphere is rejected with high confidence (i.e.  $3\sigma$ ). Primary clear atmospheric scenarios with traces of  $\text{CO}$  or  $\text{CO}_2$  have higher  $\Delta\log(\text{E})$ , remaining below the one of the flat-line model, but they cannot be rejected as firmly as the others (see also Fig. 9 in Sec. 4.2).

A primary clear atmosphere scenario was previously rejected for TRAPPIST-1 planets using HST/WFC3 G141 spectra (de Wit et al. 2018; Zhang et al. 2018; Wakeford et al. 2019). Performing the same exercise with a fixed  $10^{-3}$  water abundance for the others six TRAPPIST spectra from Zhang et al. (2018), we also confirm that a primary clear atmospheric model does not fit their spectra. We note that we simulated planet atmospheres with the same 100 layers between  $10^{-2}$  and  $10^{-5}$  even

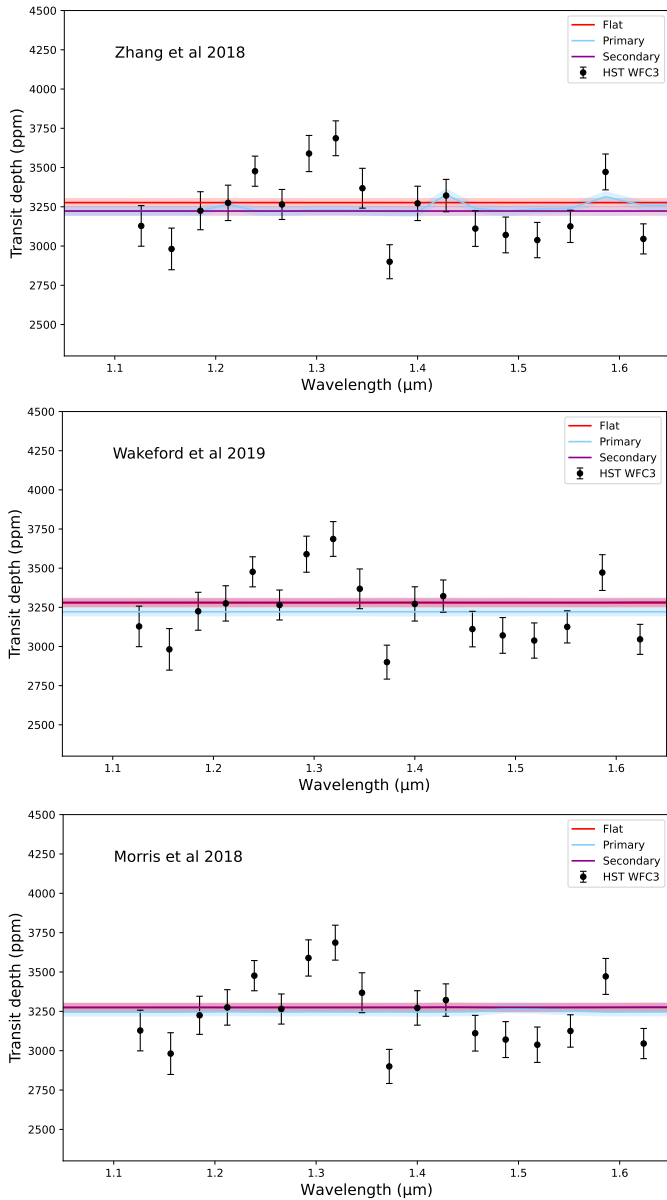


**Fig. 6.** Best fit models to TRAPPIST-1 h HST WFC3 G141 data after subtraction of stellar contamination contributions according to the Zhang et al. (2018) (top), Wakeford et al. (2019) (middle), and Morris et al. (2018) (bottom) formalism.

though they have a different size, radius, and mass. We present in Fig. 7 the best-fit atmospheric retrieval results in the case of a Hydrogen-dominated atmosphere with water as a trace gas (the volume mixing ratio was fixed to  $10^{-3}$ ) for the seven planets of the TRAPPIST-1 system. The results are presented in number of scale height and we can see that TRAPPIST-1 planets are unlikely to possess a clear atmosphere dominated by hydrogen with water in a low quantity. The comparison of logarithm evidence between a flat-line model and a primary clear atmosphere for all seven planets is detailed in appendix A.1. This is in agreement with theoretical modelling as detailed in Sec. 2.3.1 and in Turbet et al. (2020b) and Hori & Ogihara (2020).

**Table 5.** Corrected transit depth in ppm using stellar contamination models.

Wavelength ( $\mu\text{m}$ )	Transit depth (ppm)		
1.1262	3072.99	3193.93	3129.83
1.1563	2934.85	3032.81	2983.10
1.1849	3171.13	3259.82	3226.35
1.2123	3202.19	3283.50	3276.38
1.2390	3406.64	3477.46	3478.10
1.2657	3207.19	3257.41	3266.07
1.2925	3520.20	3564.16	3590.50
1.3190	3643.19	3673.80	3687.80
1.3454	3388.59	3396.28	3369.86
1.3723	2948.59	2939.83	2901.69
1.4000	3341.90	3318.92	3273.55
1.4283	3414.44	3373.99	3323.56
1.4572	3193.82	3149.00	3112.83
1.4873	3141.10	3090.15	3072.24
1.5186	3093.99	3037.20	3039.34
1.5514	3165.61	3101.84	3126.55
1.5862	3499.04	3418.90	3473.19
1.6237	3057.41	2980.84	3046.45
References	1	2	3

**References.** (1) Zhang et al. (2018); (2) Wakeford et al. (2019); (3) Morris et al. (2018)

#### 4.2. Steam atmosphere

From the review of the possible atmospheric scenario (Turbet et al. 2020b), TRAPPIST-1h could have a water-, methane-, ammonia-, nitrogen-, or even a carbon-dioxide-rich atmosphere depending on the evolution of the planet, on the species collapses, and on the photo-chemistry. A steam atmosphere is unlikely for TRAPPIST-1h as it would require the planet to have retained its atmosphere and to be stable against stellar wind (see Sec. 2.3.1). However, we tested those different hypothesis by using a similar approach as in Sec. 4.1, but allowing for heavier atmospheres by increasing the volume mixing ratio of the tested molecular absorber from 0.01 to 0.8 progressively. Best-fit atmospheric results along with derived parameters and statistical criteria are detailed in Appendix A.3. We note that some forced secondary steam atmospheric models have  $\log(E)$  equal to or slightly above the one of the flat-line model. The difference in  $\log(E)$  is above one for one case, with the CO-rich atmosphere having a volume mixing ratio fixed to 0.2. This model has a  $\Delta\log(E)$  of 1.01 corresponding to  $2.1\sigma$  confidence, hence a 'weak detection' in Benneke & Seager (2013) classification. The best-fit spectrum of the models presenting an elevated  $\log(E)$  are plotted in Fig. 8. They correspond to the model of 20%  $\text{CO}_2$  and 80% of  $\text{N}_2$  and  $\text{NH}_3$ . Carbon dioxide and carbon monoxide have similar absorption features in the HST/WFC3 wavelength range, which leads to similar best-fit results. Moreover, as the features are very small, we obtained the same volume mixing ratios for those species. We note that  $\text{N}_2$  acts as a fill gas in the atmosphere as it does not have features; the best-fit spectrum is then similar to that of the flat line. We can add a CO-rich atmosphere to the possible atmospheric scenario for TRAPPIST-1h.

We note that  $\Delta\log(E)$  remains below one for most of the other tested models, meaning that they are not statistically significant. We present in Fig. 9 the comparison of the log evidence for a flat line to that of single molecule retrievals from the primary clear analysis of Sec. 4.1 and the secondary models of Sec. 4.2 follow-



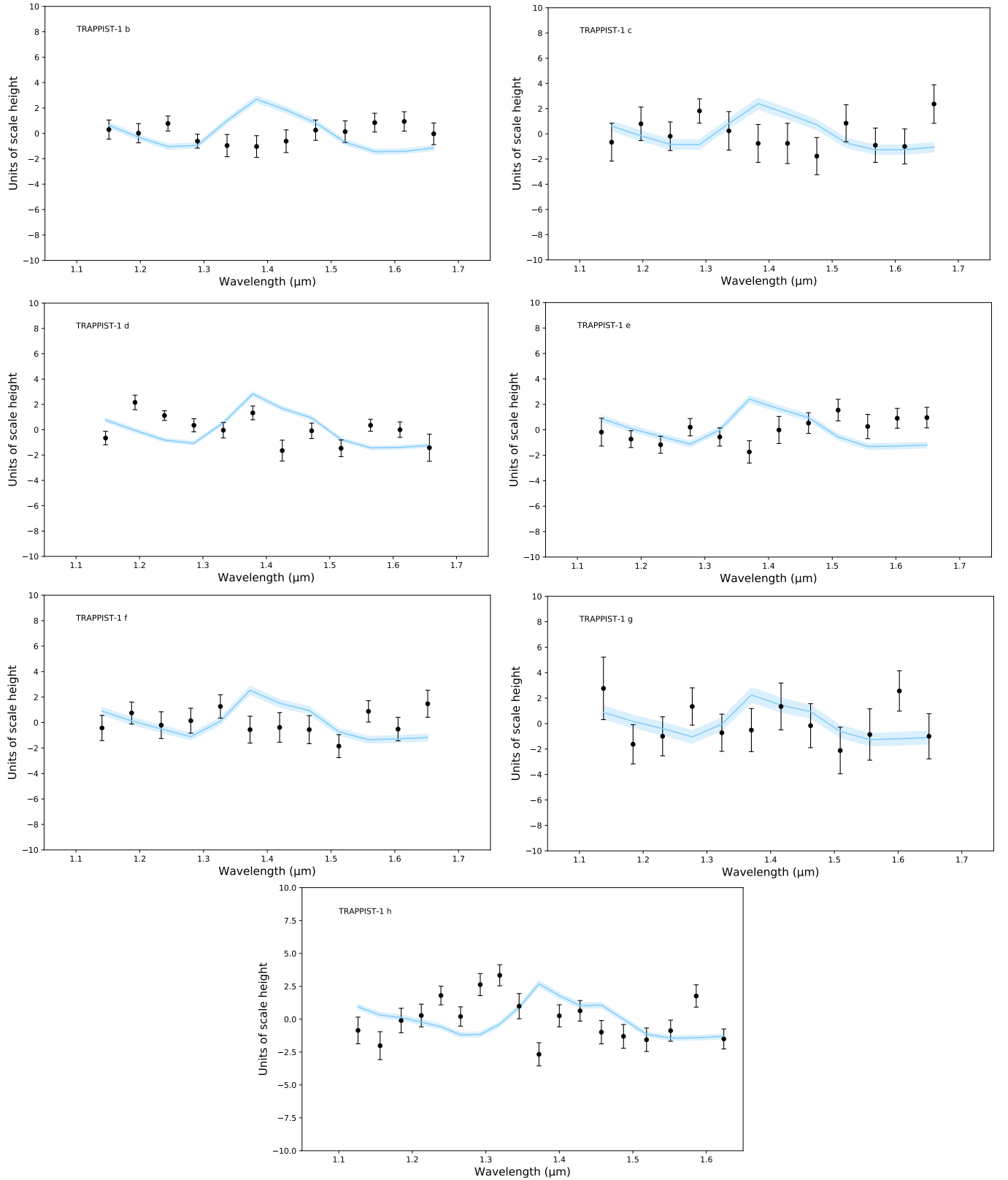


**Fig. 7.** Comparison of the best-fit atmospheric results for TRAPPIST-1 planetary spectra in the case of a forced primary clear atmosphere with a volume mixing ratio of water fixed to  $10^{-3}$  in a H-dominated atmosphere. We used spectra from Zhang et al. (2018) for the TRAPPIST-1 b to g retrievals and present the results in units of scale height.

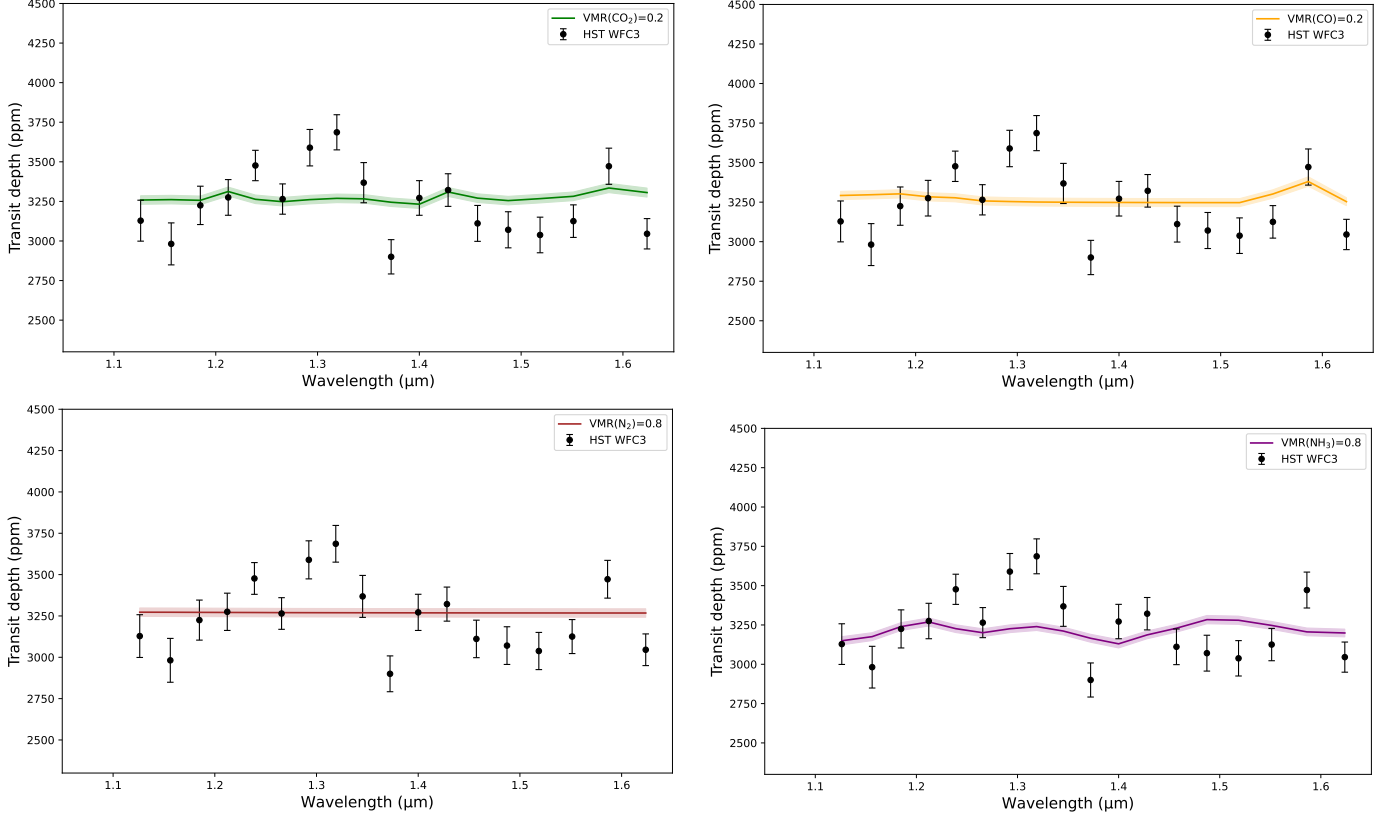
ing the formalism of Fig.6 in Mugnai et al. (2021). We decided to represent the  $\Delta\log(E)$  with respect to the mean molecular weight of the modelled atmospheres to compare the different scenarios

as similar molecular abundances could lead to different weights and metallicities. Primary atmospheric models with a metallicity below 50 times solar (i.e.  $\text{mmw}=2.70$  g/mol) are rejected with

**Table 6.** Best-fit atmospheric results and derived parameters for a primary clear retrieval analysis.

Model	$R_p(R_\oplus)$	T(K)	$\mu(\text{g/mol})$	H(km)	$\chi^2$	$\tilde{\chi}^2$	log(E)	$\Delta\log(E)$
Flat-line	$0.61 \pm 0.110$	$296 \pm 225$	2.30	71.28	64.95	3.61	110.55	N/A
H <sub>2</sub> O	$0.70 \pm 0.003$	$140 \pm 2$	2.32	75.27	128.68	7.15	74.78	-35.77
CO <sub>2</sub>	$0.71 \pm 0.003$	$157 \pm 26$	2.35	86.84	68.37	3.80	108.99	-1.56
CO	$0.72 \pm 0.003$	$158 \pm 25$	2.33	88.84	70.53	3.92	107.93	-2.62
CH <sub>4</sub>	$0.69 \pm 0.003$	$139 \pm 2$	2.32	72.20	146.35	8.13	65.48	-45.07
NH <sub>3</sub>	$0.68 \pm 0.003$	$140 \pm 3$	2.32	70.56	107.58	5.98	85.38	-25.17
N <sub>2</sub>	$0.72 \pm 0.003$	$156 \pm 26$	2.33	87.85	69.71	3.87	106.82	-3.73

**Notes.** The primary clear atmospheric scenario was simulated including the molecular absorption with a volume mixing ratio fixed to  $10^{-3}$  in a H-dominated atmosphere.

**Fig. 8.** Comparison of the best-fit atmospheric results for the TRAPPIST-1h spectrum in the case of four forced secondary clear atmospheres with a volume mixing ratio of CO<sub>2</sub> fixed to 0.2 (upper left), CO to 0.2 (upper right), N<sub>2</sub> to 0.8 (bottom left), and ammonia to 0.8 (bottom right).

more than  $5\sigma$  confidence (i.e. the Bayes factor is inferior to -11), except for CO and CO<sub>2</sub>. In addition, if the atmosphere was primary, it would be unlikely that it does not contain any water. The equivalence between abundances, the mean molecular weight, and solar metallicity is presented in Appendix Table A.3 and a figure of all  $\Delta\log(E)$  with respect to the abundances is presented in Appendix B.11. The area between dashes represents the set of Bayes factor values for which it is not possible to conclude compared to a flat line, that is with absolute  $\Delta\log(E)$  below 3. Models with a  $\Delta\log(E)$  between -3 and -11 can be significantly rejected compared to a flat line, while the ones below -11 are strongly disfavoured.

#### 4.3. Impact of changing the spectral resolution

Neither stellar contamination nor atmospheric absorption can explain the rise in the transit depth around  $1.3 \mu\text{m}$ . This is proba-

bly due to scattering noise remaining after the extraction and the spectral light curve fitting. By changing the resolution of the data extraction, we investigated if the scattering at  $1.3 \mu\text{m}$  remains significant and if a single narrow band of the spectrum caused this 'feature'. We performed the same data analysis as in Sec. 3.1 using two other binning resolutions with a resolving power of 25 and 70 around  $1.4 \mu\text{m}$ , respectively. We also performed the same retrieval analysis using the primary, the secondary, and the flat-line set-ups on the two spectra. We obtained similar results; the flat-line model is the best fit according to the Bayes factor.

We present in Fig.10 the best-fit atmospheric results on the two spectra of TRAPPIST-1 h. The log(E) of the flat line is 47.52 and 163.62 for the very low and the high resolution spectra whereas the log(E) of the primary model reaches 47.04 and 163.15, respectively. Log(E) of the secondary model are also below the one of the flat-line model, that is 47.42 and 163.42. Changing the resolution of the spectrum does not flatten or increase the rise of the transit depth at  $1.3 \mu\text{m}$  and it was recovered

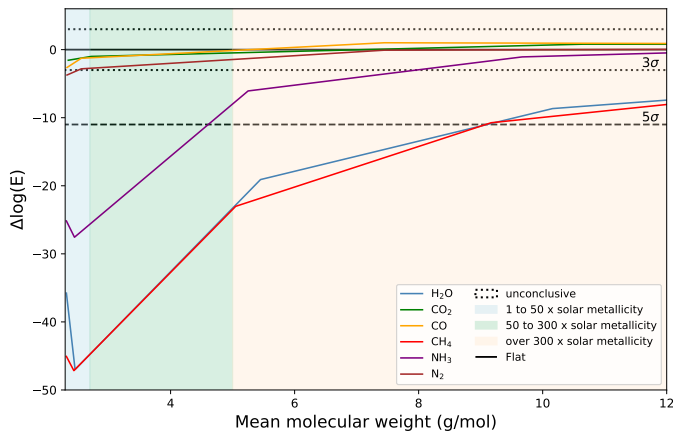


**Fig. 9.** Comparison of the log evidence for a flat line to that of single molecule retrievals where the abundance of the molecule is fixed and no clouds were included. We represent the Delta log(E) with respect to the mean molecular weight of the tested atmospheres. The region between dashes represents the set of Bayes factor values for which it is not possible to conclude compared to a flat line, that is with absolute  $\Delta\log(E)$  below 3. Models below the large dashed lines are strongly disfavoured compared to the flat line.

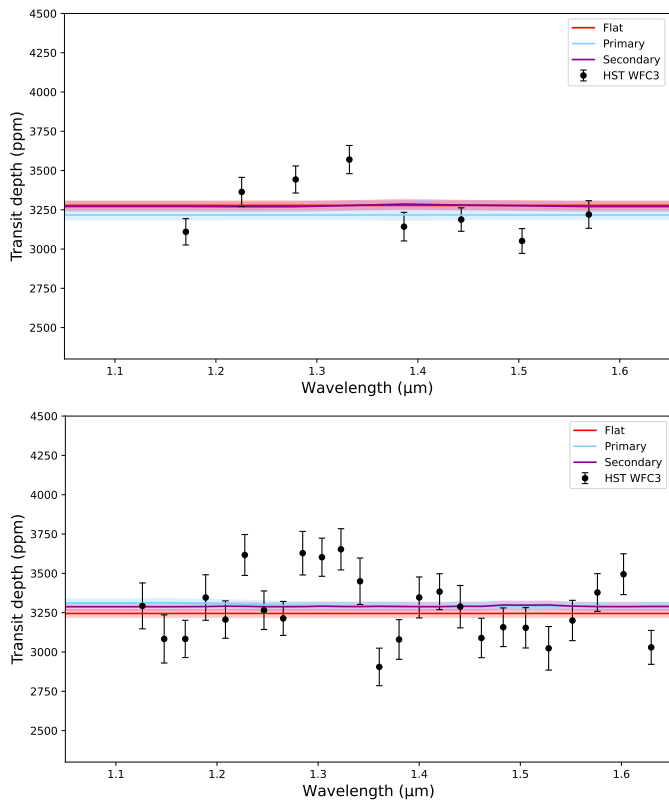


**Fig. 10.** Best fit models to TRAPPIST-1 h HST WFC3 G141 data using a very low (top) and a high (bottom) resolution with a resolving power of 25 and 70 around  $1.4\mu\text{m}$ .

in each case. Results from Sec. 3.2 are confirmed while using different resolutions. A flat-line model remains the best-fit to the TRAPPIST-1 h spectrum.

## 5. Conclusion

Terrestrial planets with a secondary envelope are challenging to characterise especially given the low resolution and narrow wavelength coverage of HST. Here, we have presented a transmission spectrum of a  $0.7 R_{\oplus}$  planet, TRAPPIST-1h, the seventh planet of the highly studied TRAPPIST-1 system. This planet is the furthest and the smallest planet of the system, yet we were able to obtain a spectrum by combining three different HST observations. We cannot make a strong claim from the analysis of the spectrum as it is better fitted using a flat line. However, we were able to rule out with more than  $3\sigma$  confidence a primary clear atmosphere, as for the other TRAPPIST planets. Given these observations, we are not yet able to distinguish between a featureless cloudy H-dominated atmosphere and a clear or cloudy secondary envelope with smaller spectral features. The two models have similar statistical significance and cannot be distinguished from retrieval analysis. We cannot completely rule out the possibility that TRAPPIST-1h has lost its atmosphere over its lifetime either as the evidence for a flat-line model is favoured. We tested secondary clear atmospheric scenarios and found that a CO-rich atmosphere with a volume mixing ratio of 0.2 in an hydrogen atmosphere obtained the best statistical result with a Bayes factor of 1.01 (i.e. a  $2.1\sigma$  detection). Yet this result is not significant enough and is mostly driven by the last points of the spectrum. This could be due to stellar activity even though all the stellar contamination models tested here were not able to reproduce those points and the rise of the transit depth around  $1.3\mu\text{m}$ . Other absorbing species, such as  $\text{H}_2\text{S}$  or  $\text{H}_2\text{CO}$ , could also create features around  $1.3\mu\text{m}$ , but they are unlikely to be produced in the TRAPPIST-1 h atmosphere with such a high level of absorption. The feature is likely caused by either stellar contamination, or by the planet. However, as previously stated in this paper, we cannot find an explanation for it. We note that the while these scatter data points will cause the atmospheric model to be poorly fit, the same is true of the flat and cloudy models. Therefore, as each will feature these points equally poorly, the evidence between the two will be independent of this and so not overly affected. Future observations with the James Webb Space Telescope (JWST) will hopefully remove the ambiguity; however, as shown in Fig. 9, we can rule out clear H/He atmospheres with high confidence. It is then necessary to obtain more data on this planet and on the other six planets of the system to prove the presence of an atmosphere and better constrain the nature of this intriguing planetary system.

**Acknowledgements.** This study makes use of observations with the NASA/ESA Hubble Space Telescope, obtained at the Space Telescope Science Institute (STScI) operated by the Association of Universities for Research in Astronomy. The publicly available HST observations presented here were taken as part of proposal 15304, led by Julien de Wit. These were obtained from the Hubble Archive which is part of the Mikulski Archive for Space Telescopes.

## References

- Abel, M., Frommhold, L., Li, X., & Hunt, K. L. 2011, The Journal of Physical Chemistry A, 115, 6805
- Abel, M., Frommhold, L., Li, X., & Hunt, K. L. 2012, The Journal of chemical physics, 136, 044319
- Al-Refaie, A. F., Changeat, Q., Venot, O., Waldmann, I. P., & Tinetti, G. 2021, A comparison of chemical models of exoplanet atmospheres enabled by TauREx 3.1
- Al-Refaie, A. F., Changeat, Q., Waldmann, I. P., & Tinetti, G. 2021, ApJ, 917, 37
- Arney, G., Domagal-Goldman, S. D., Meadows, V. S., et al. 2016, Astrobiology, 16, 873–899
- Benneke, B. & Seager, S. 2013, The Astrophysical Journal, 778, 153

- Bolmont, E., Selsis, F., Owen, J. E., et al. 2017, *Monthly Notices of the Royal Astronomical Society*, 464, 3728–3741
- Bourrier, V., Ehrenreich, D., Wheatley, P. J., et al. 2017a, *Astronomy & Astrophysics*, 599, L3
- Bourrier, V., Wit, J. d., Bolmont, E., et al. 2017b, *The Astronomical Journal*, 154, 121
- Burdanov, A. Y., Lederer, S. M., Gillon, M., et al. 2019, *Monthly Notices of the Royal Astronomical Society*, 487, 1634–1652
- Burgasser, A. J. & Mamajek, E. E. 2017, *The Astrophysical Journal*, 845, 110
- Chubb, K. L., Rocchetto, M., Yurchenko, S. N., et al. 2021, *Astronomy & Astrophysics*, 646, A21
- Claret, A. 2018, *Astronomy & Astrophysics*, 618, A20
- Claret, A., Hauschildt, P. H., & Witte, S. 2012, *Astronomy & Astrophysics*, 546, A14
- Claret, A., Hauschildt, P. H., & Witte, S. 2013, *Astronomy & Astrophysics*, 552, A16
- Coleman, G. A. L., Leleu, A., Alibert, Y., & Benz, W. 2019, *Astronomy & Astrophysics*, 631, A7
- de Wit, J., Wakeford, H. R., Gillon, M., et al. 2016, *Nature*, 537, 69–72
- de Wit, J., Wakeford, H. R., Lewis, N. K., et al. 2018, *Nature Astronomy*, 2, 214–219
- Delrez, L., Gillon, M., Triaud, A. H. M. J., et al. 2018, *Monthly Notices of the Royal Astronomical Society*, 475, 3577–3597
- Deming, D., Wilkins, A., McCullough, P., et al. 2013, *The Astrophysical Journal*, 774, 17
- Dencs, Z. & Regály, Z. 2019, *Monthly Notices of the Royal Astronomical Society*, 487, 2191–2199
- Dobos, V., Barr, A. C., & Kiss, L. L. 2019, *Astronomy & Astrophysics*, 624, A2
- Dong, C., Huang, Z., & Lingam, M. 2019, *The Astrophysical Journal*, 882, L16
- Dong, C., Jin, M., Lingam, M., et al. 2018, *Proceedings of the National Academy of Sciences*, 115, 260–265
- Dong, C., Lingam, M., Ma, Y., & Cohen, O. 2017, *The Astrophysical Journal*, 837, L26
- Ducrot, E., Gillon, M., Delrez, L., et al. 2020, *Astronomy & Astrophysics*, 640, A112
- Ducrot, E., Sestovic, M., Morris, B. M., et al. 2018, *The Astronomical Journal*, 156, 218
- Edwards, B., Changeat, Q., Mori, M., et al. 2021, *The Astronomical Journal*, 161, 44
- Feroz, F., Hobson, M. P., & Bridges, M. 2009, *Monthly Notices of the Royal Astronomical Society*, 398, 1601–1614
- Fletcher, L. N., Gustafsson, M., & Orton, G. S. 2018, *The Astrophysical Journal Supplement Series*, 235, 24
- Foreman-Mackey, D., Hogg, D. W., Lang, D., & Goodman, J. 2013, *Publications of the Astronomical Society of the Pacific*, 125, 306–312
- Gao, P., Hu, R., Robinson, T. D., Li, C., & Yung, Y. L. 2015, *The Astrophysical Journal*, 806, 12
- Gillon, M., Bonfils, X., Demory, B.-O., et al. 2011, *Astronomy & Astrophysics*, 525, A32
- Gillon, M., Jehin, E., Lederer, S. M., et al. 2016, *Nature*, 533, 221–224
- Gillon, M., Triaud, A. H. M. J., Demory, B.-O., et al. 2017, *Nature*, 542, 456–460
- Gillon, M., Triaud, A. H. M. J., Jehin, E., et al. 2013, *Astronomy & Astrophysics*, 555, L5
- Grimm, S. L., Demory, B.-O., Gillon, M., et al. 2018, *Astronomy & Astrophysics*, 613, A68
- Hori, Y. & Ogihara, M. 2020, *The Astrophysical Journal*, 889, 77
- Hu, R., Peterson, L., & Wolf, E. T. 2020, *The Astrophysical Journal*, 888, 122
- Kass, R. E. & Raftery, A. E. 1995, *Journal of the American Statistical Association*, 90, 773
- Kasting, J. F., Whitmire, D. P., & Reynolds, R. T. 1993, *Icarus*, 101
- Kimura, T. & Ikoma, M. 2020, *MNRAS*, 496, 3755
- Kral, Q., Wyatt, M. C., Triaud, A. H. M. J., et al. 2018, *Monthly Notices of the Royal Astronomical Society*, 479, 2649–2672
- Kreidberg, L., Bean, J. L., Désert, J.-M., et al. 2014, *Nature*, 505, 69–72
- Lammer, H., Selsis, F., Ribas, I., et al. 2003, *The Astrophysical Journal*, 598, L121
- Lincowski, A. P., Lustig-Yaeger, J., & Meadows, V. S. 2019, *The Astronomical Journal*, 158, 26
- Lincowski, A. P., Meadows, V. S., Crisp, D., et al. 2018, *The Astrophysical Journal*, 867, 76
- Luger, R., Lustig-Yaeger, J., & Agol, E. 2017a, *The Astrophysical Journal*, 851, 94
- Luger, R., Sestovic, M., Kruse, E., et al. 2017b, *Nature Astronomy*, 1
- MacDonald, M. G. & Dawson, R. I. 2018, *The Astronomical Journal*, 156, 228
- Makarov, V. V., Berghea, C. T., & Efroimsky, M. 2018, *The Astrophysical Journal*, 857, 142
- Moran, S. E., Hörst, S. M., Batalha, N. E., Lewis, N. K., & Wakeford, H. R. 2018, *The Astronomical Journal*, 156, 252
- Morello, G., Claret, A., Martin-Lagarde, M., et al. 2020, *The Astronomical Journal*, 159, 75
- Morris, B. M., Agol, E., Davenport, J. R. A., & Hawley, S. L. 2018, *The Astrophysical Journal*, 857, 39
- Mugnai, L. V., Modirrousta-Galian, D., Edwards, B., et al. 2021, *The Astronomical Journal*, 161, 284
- Ormel, C. W., Liu, B., & Schoonenberg, D. 2017, *Astronomy & Astrophysics*, 604, A1
- Papaloizou, J. C. B., Szuszkiewicz, E., & Terquem, C. 2018, *Monthly Notices of the Royal Astronomical Society*, 476, 5032–5056
- Pierrehumbert, R. & Gaidos, E. 2011, *The Astrophysical Journal*, 734, L13
- Polyansky, O. L., Kyuberis, A. A., Zobov, N. F., et al. 2018, *Monthly Notices of the Royal Astronomical Society*, 480, 2597–2608
- Rackham, B. V., Apai, D., & Giampapa, M. S. 2018, *The Astrophysical Journal*, 853, 122
- Ramirez, R. M. & Kaltenegger, L. 2014, *The Astrophysical Journal*, 797, L25
- Ramirez, R. M. & Kaltenegger, L. 2017, *The Astrophysical Journal*, 837, L4
- Rothman, L. S., Gamache, R. R., Goldman, A., et al. 1987, *Appl. Opt.*, 26, 4058
- Rothman, L. S., Gordon, I. E., Babikov, Y., et al. 2013, *J. Quant. Spectr. Rad. Transf.*, 130, 4
- Rothman, L. S., Gordon, I. E., Barber, R. J., et al. 2010, *J. Quant. Spectr. Rad. Transf.*, 111, 2139
- Rugheimer, S., Segura, A., Kaltenegger, L., & Sasselov, D. 2015, *The Astrophysical Journal*, 806, 137
- Sagan, C. & Chyba, C. 1997, *Science*, 276, 1217
- Tamayo, D., Rein, H., Petrovich, C., & Murray, N. 2017, *The Astrophysical Journal*, 840, L19
- Tennyson, J. & Yurchenko, S. 2018, *Atoms*, 6, 26
- Tennyson, J., Yurchenko, S. N., Al-Refaie, A. F., et al. 2016, *Journal of Molecular Spectroscopy*, 327, 73–94
- Tian, F. D. & Ida, S. 2015, *Nature Geoscience*, 8, 177
- Trotta, R. 2008, *Contemporary Physics*, 49, 71–104
- Tsiaras, A., Rocchetto, M., Waldmann, I. P., et al. 2016a, *The Astrophysical Journal*, 820, 99
- Tsiaras, A., Waldmann, I. P., Rocchetto, M., et al. 2016b, *The Astrophysical Journal*, 832, 17
- Tsiaras, A., Waldmann, I. P., Zingales, T., et al. 2018, *The Astronomical Journal*, 155, 156
- Turbet, M., Bolmont, E., Bourrier, V., et al. 2020a, *Space Science Reviews*, 216
- Turbet, M., Bolmont, E., Ehrenreich, D., et al. 2020b, *Astronomy & Astrophysics*, 638, A41
- Turbet, M., Bolmont, E., Leconte, J., et al. 2018, *Astronomy & Astrophysics*, 612, A86
- Turbet, M., Ehrenreich, D., Lovis, C., Bolmont, E., & Fauchez, T. 2019a, *Astronomy & Astrophysics*, 628, A12
- Turbet, M., Tran, H., Perali, O., et al. 2019b, *Icarus*, 321, 189–199
- Vida, K., Kővári, Z., Pál, A., Oláh, K., & Kriskovics, L. 2017, *The Astrophysical Journal*, 841, 124
- Vidal-Madjar, A., Lecavelier des Etangs, A., Désert, J. M., et al. 2003, *Nature*, 422
- Wakeford, H. R., Lewis, N. K., Fowler, J., et al. 2019, *The Astronomical Journal*, 157, 11
- Wheatley, P. J., Louden, T., Bourrier, V., Ehrenreich, D., & Gillon, M. 2017, *Monthly Notices of the Royal Astronomical Society: Letters*, 465, L74–L78
- Wolf, E. T. & Toon, O. B. 2010, *Science*, 328, 1266
- Wordsworth, R., Kalugina, Y., Lokshantov, S., et al. 2017, *Geophysical Research Letters*, 44, 665–671
- Wordsworth, R. D., Schaefer, L. K., & Fischer, R. A. 2018, *The Astronomical Journal*, 155, 195
- Yip, K. H., Changeat, Q., Edwards, B., et al. 2020, *The Astronomical Journal*, 161, 4
- Yurchenko, S. N., Barber, R. J., & Tennyson, J. 2011, *Monthly Notices of the Royal Astronomical Society*, 413, 1828–1834
- Yurchenko, S. N. & Tennyson, J. 2014, *Monthly Notices of the Royal Astronomical Society*, 440, 1649–1661
- Zhang, Z., Zhou, Y., Rackham, B. V., & Apai, D. 2018, *The Astronomical Journal*, 156, 178

## Appendix A: Additional tables

**Table A.1.** Best-fit logarithm evidence of a flat-line and a primary clear model for the seven planets of the TRAPPIST-1 system.

Model	Flat-line	Primary clear
TRAPPIST-1 b	76.54	45.37
TRAPPIST-1 c	77.42	68.28
TRAPPIST-1 d	71.92	37.84
TRAPPIST-1 e	82.16	58.06
TRAPPIST-1 f	79.58	65.72
TRAPPIST-1 g	79.73	75.73
TRAPPIST-1 h	110.55	74.78

**Notes.** The primary clear atmospheric scenario was simulated including  $\text{H}_2\text{O}$  with a volume mixing ratio fixed to  $10^{-3}$  in a H-dominated atmosphere for all seven planets of the TRAPPIST-1 system.

**Table A.2.** Statistical results of the stellar contamination modelling on combined TRAPPIST-1h HST WFC3 G141 data and the K2 photometry value from Luger et al. (2017a).

Model	$\chi^2$	$\tilde{\chi}^2$
Flat-line	72.14	3.80
Stellar Zhang et al. (2018)	73.74	3.81
Stellar Wakeford et al. (2019)	197.75	10.15
Stellar Morris et al. (2018)	99.37	5.23

**Notes.** Chi-squared ( $\chi^2$ ) and reduced chi-squared ( $\tilde{\chi}^2$ ) were computed using the result of the stellar contamination models.

## Appendix B: Additional figures

**Table A.3.** Best-fit atmospheric results and derived parameters for secondary retrieval analysis.

Model	$R_p(R_\oplus)$	T(K)	$\mu(\text{g/mol})$	H(km)	met (x solar)	$\chi^2$	$\tilde{\chi}^2$	log(E)	$\Delta\log(E)$
Flat-line	$0.61\pm0.11$	$296\pm225$	2.30	71.28	1	64.95	3.61	110.55	N/A
VMR( $\text{H}_2\text{O}$ )									
0.01	$0.69\pm0.003$	$139\pm2$	2.46	69.09	20	150.67	8.37	63.55	-47.00
0.2	$0.71\pm0.003$	$142\pm6$	5.45	32.98	350	97.25	5.40	91.46	-19.09
0.5	$0.72\pm0.003$	$147\pm15$	10.16	18.78	900	78.43	4.35	101.89	-8.66
0.8	$0.72\pm0.003$	$153\pm24$	14.87	13.50	1400	72.92	4.05	105.07	-5.48
VMR( $\text{CO}_2$ )									
0.01	$0.71\pm0.003$	$155\pm22$	2.72	73.68	50	64.22	3.57	109.55	-1.00
0.2	$0.72\pm0.003$	$173\pm24$	10.65	21.48	950	63.69	3.54	111.35	0.80
0.5	$0.72\pm0.003$	$174\pm24$	23.16	10.03	2400	63.93	3.55	111.26	0.71
0.8	$0.73\pm0.003$	$174\pm25$	35.67	6.54	3800	64.30	3.57	110.98	0.43
VMR( $\text{CO}$ )									
0.01	$0.72\pm0.003$	$159\pm27$	2.56	81.36	30	68.36	3.80	109.28	-1.27
0.2	$0.72\pm0.003$	$174\pm24$	7.45	31.19	600	63.23	3.51	111.56	1.01
0.5	$0.73\pm0.003$	$175\pm26$	15.16	15.45	1500	63.64	3.54	111.38	0.83
0.8	$0.73\pm0.003$	$174\pm24$	22.87	10.21	2300	63.97	3.55	111.15	0.60
VMR( $\text{CH}_4$ )									
0.01	$0.68\pm0.003$	$139\pm3$	2.44	66.32	20	170.07	9.45	63.39	-47.16
0.2	$0.69\pm0.003$	$141\pm5$	5.05	33.60	300	104.28	5.79	87.53	-23.02
0.5	$0.70\pm0.003$	$145\pm12$	9.17	19.87	800	81.64	4.54	99.81	-10.74
0.8	$0.71\pm0.004$	$150\pm18$	13.30	14.43	1300	74.92	4.16	103.72	-6.83
VMR( $\text{NH}_3$ )									
0.01	$0.66\pm0.003$	$140\pm3$	2.45	63.82	20	112.31	6.24	82.99	-27.56
0.2	$0.69\pm0.004$	$145\pm11$	5.25	33.95	350	72.48	4.03	104.48	-6.07
0.5	$0.70\pm0.005$	$158\pm26$	9.67	20.39	850	67.57	3.75	109.48	-1.07
0.8	$0.71\pm0.004$	$168\pm26$	14.09	15.11	1500	65.14	3.62	110.59	0.04
VMR( $\text{N}_2$ )									
0.01	$0.72\pm0.003$	$159\pm27$	2.56	81.54	30	71.67	3.98	107.73	-2.82
0.2	$0.73\pm0.003$	$171\pm25$	7.45	30.78	600	65.33	3.63	110.47	-0.08
0.5	$0.73\pm0.003$	$174\pm24$	15.16	15.36	1500	64.96	3.61	110.67	0.12
0.8	$0.73\pm0.003$	$171\pm25$	22.87	10.05	2300	64.72	3.59	110.72	0.17

**Notes.** Secondary atmospheric scenarios were simulated including molecular absorption with a fixed volume mixing ratio increasing progressively from 0.01 to 0.8.

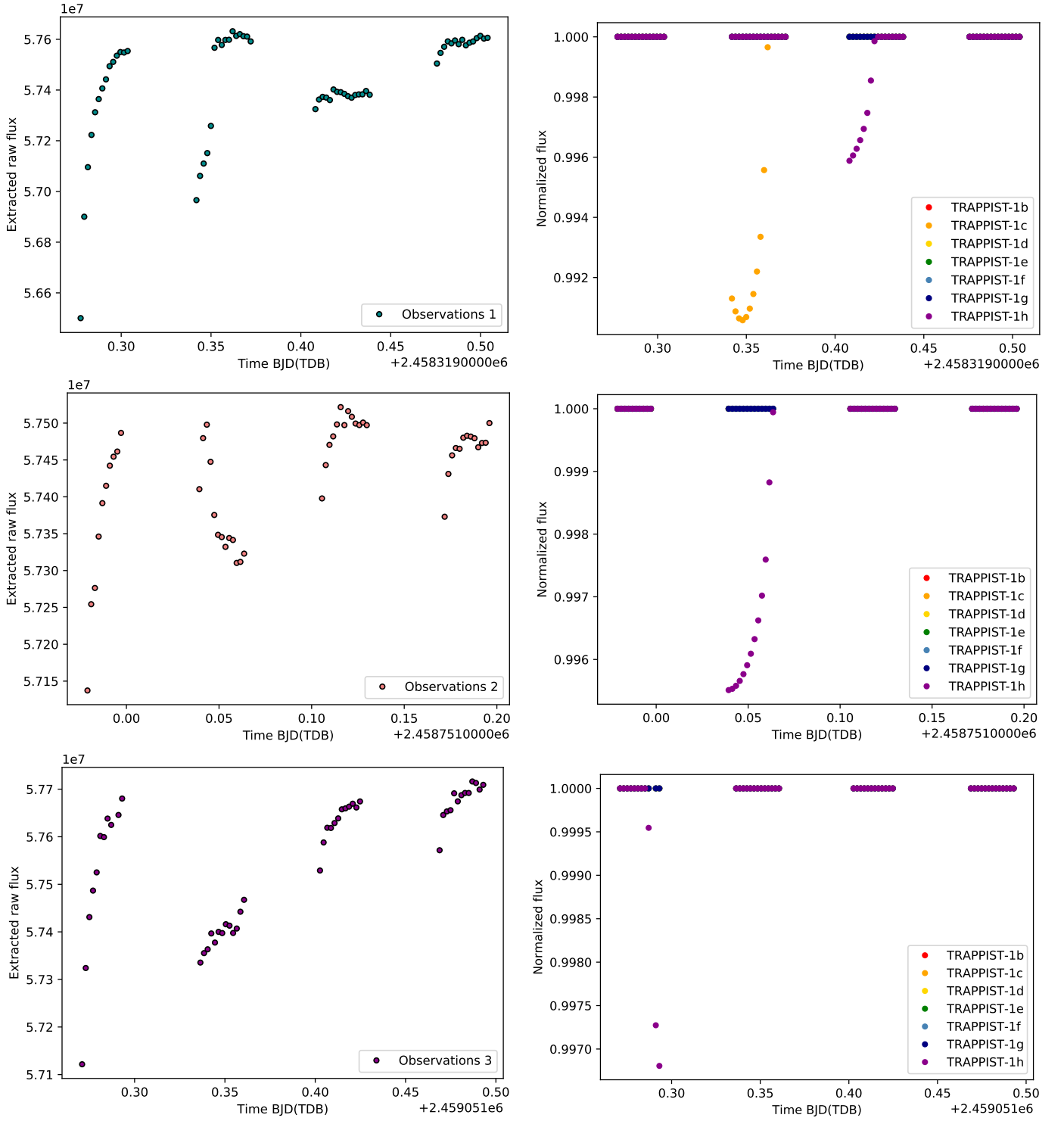


**Fig. B.1.** Left: Raw extracted light curves for the TRAPPIST-1h observations (top: Observations 1 July 2017, middle: Observations 2 September 2019, and bottom Observations 3: July 2020). Right: Predicted planetary transits using PyLightcurve transits model and Gillon et al. (2017) system parameters at the time of the observations.



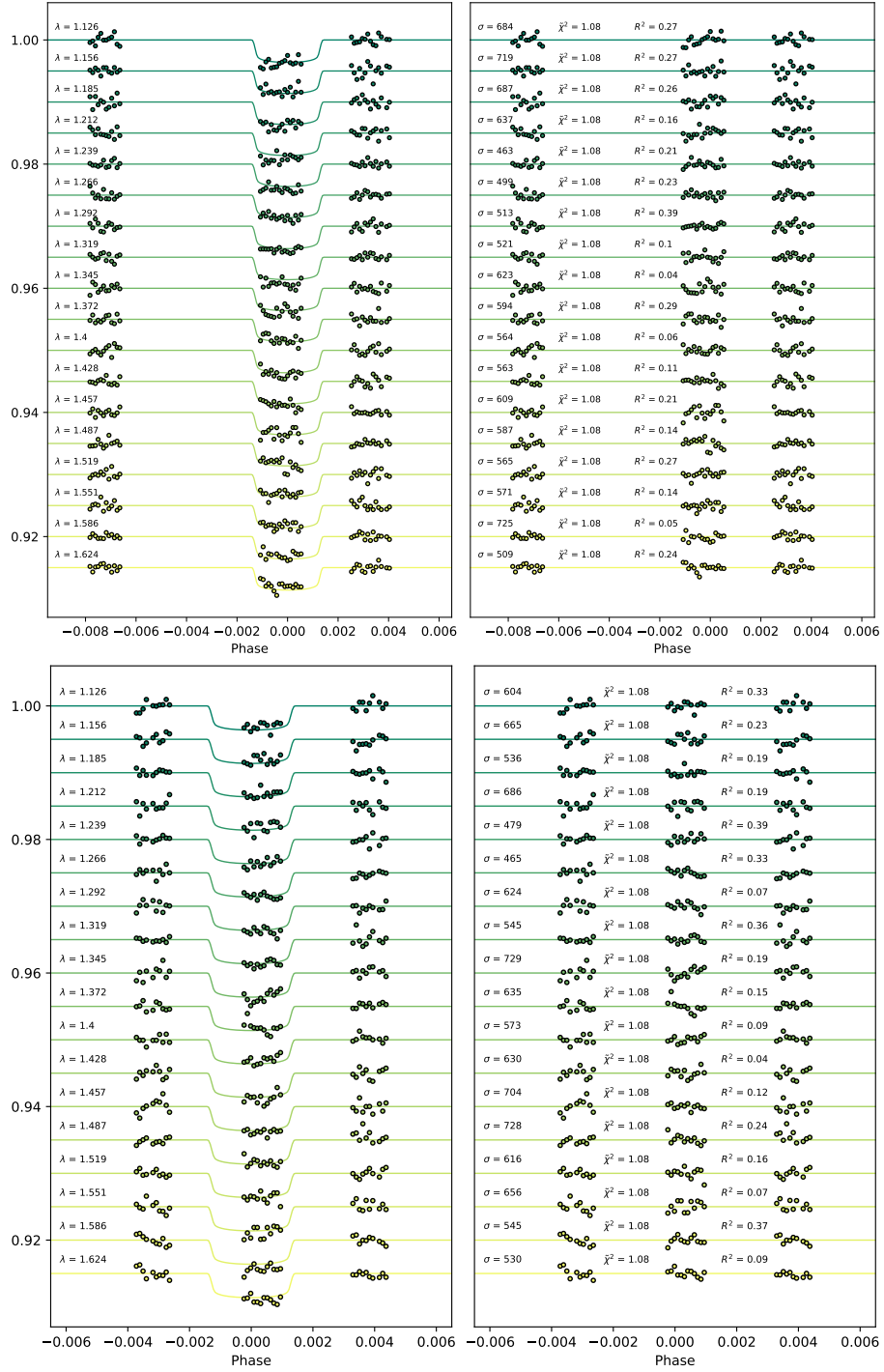


**Fig. B.2.** Spectral light curve fits of the July 2017 (top) and 2020 (bottom) visits (Observation 1 and 3) for the transmission spectra of TRAPPIST-1H. An artificial offset in the y-axis has been applied for clarity. For each light curve, the left panel shows the de-trended spectral light curves with the best fit model in dotted lines with the centred wavelength, and the right panel shows the residuals and values for the standard deviation ( $\sigma$ ) in ppm, the reduced Chi-squared ( $\chi^2$ ), and the auto-correlation ( $R^2$ ).

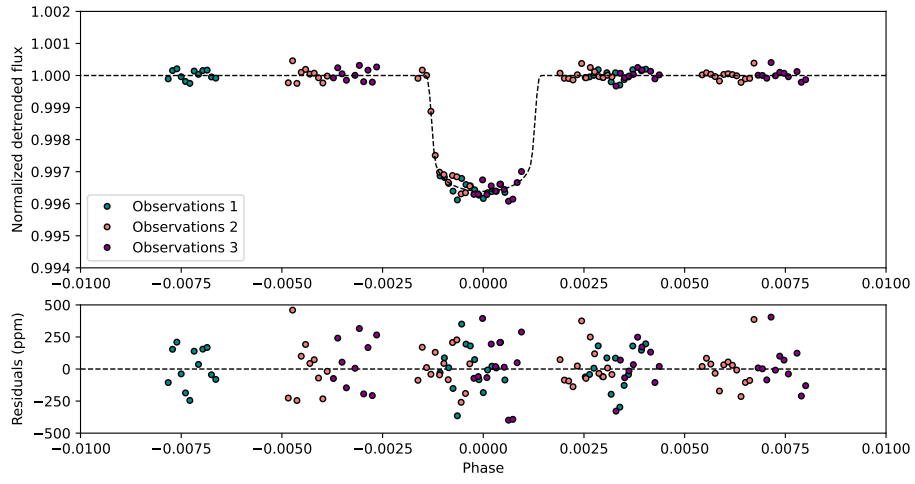


**Fig. B.3.** White light curve fits for the three visits on TRAPPIST-1h (top). The transit model (dotted line) was simulated using a weighted mean of the three observations' planet-to-star radius ratios, i.e. 0.0572.

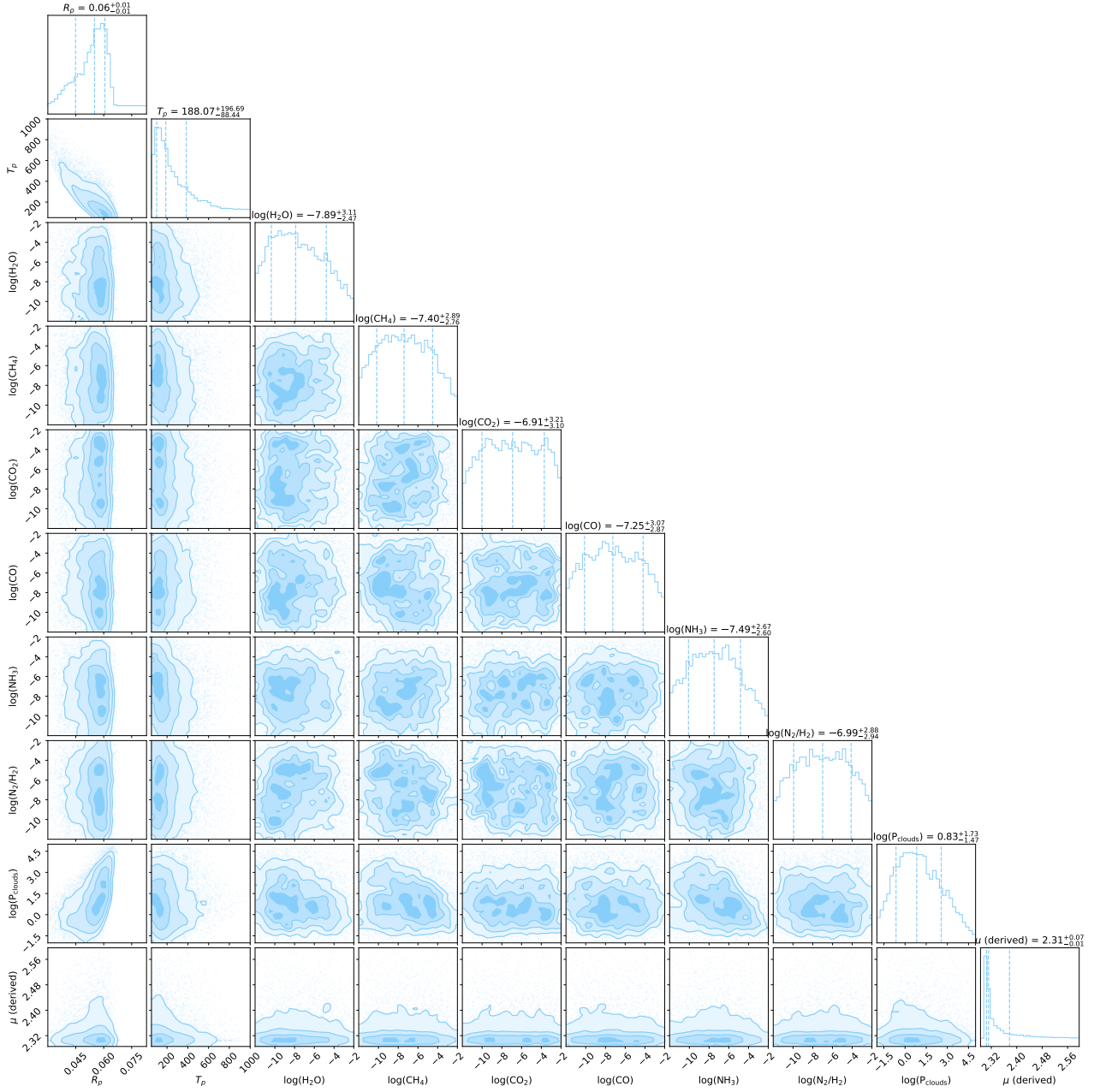


**Fig. B.4.** Posterior distributions for the primary atmospheric retrieval on the extracted TRAPPIST-1h spectrum.

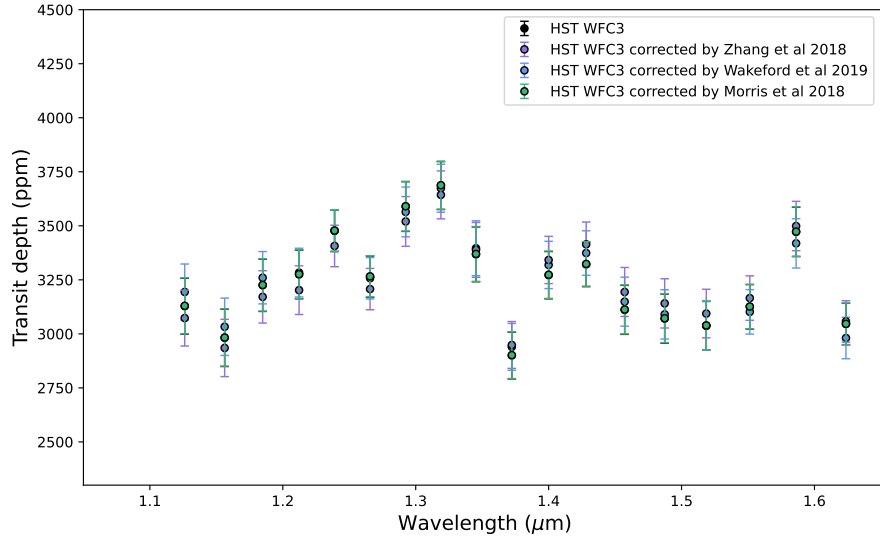


**Fig. B.5.** Combined transit depth in ppm using the three HST/WFC3 G141 transit observations and corrected transit depth using stellar contamination models from Zhang et al. (2018) (purple), Wakeford et al. (2019) (blue), and Morris et al. (2018) (green). The latter (in green) and the raw extracted spectrum (in black) are almost similar because the stellar contribution of Morris et al. (2018) is flat in the HST/WFC3 NIR wavelength range.

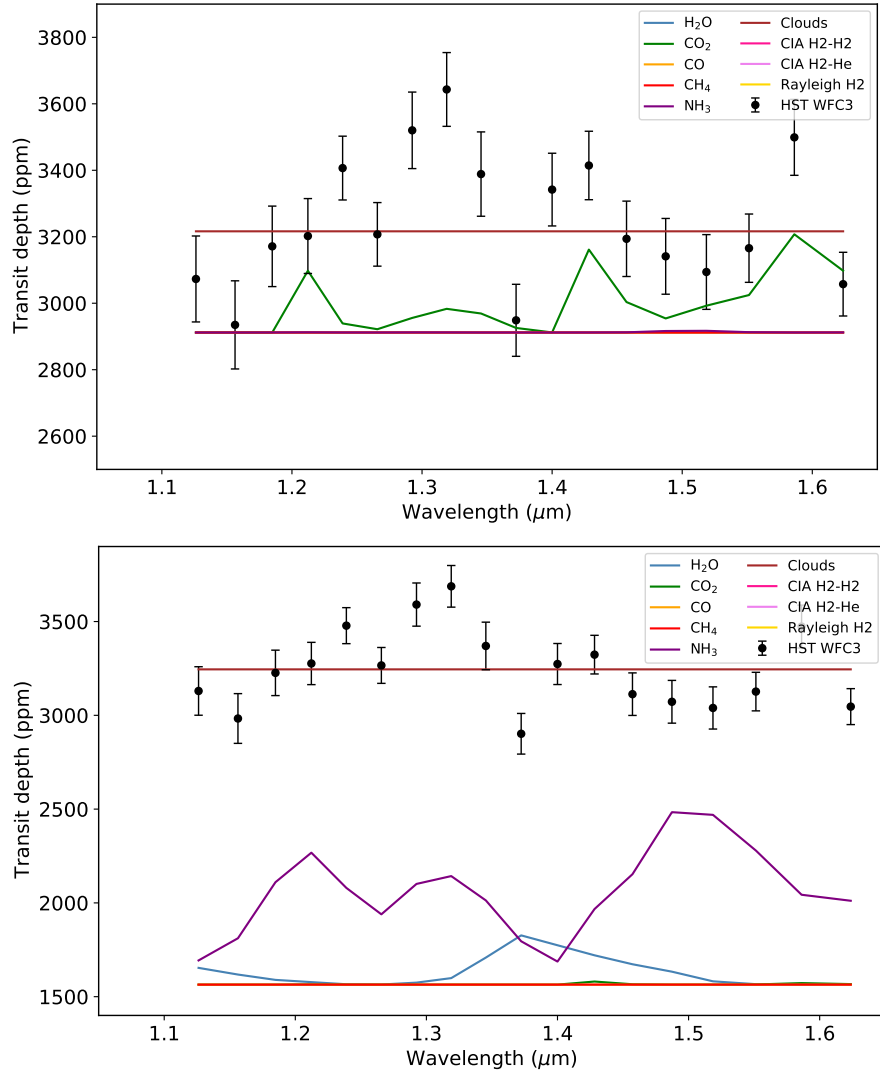


**Fig. B.6.** Opacity contributions from the primary best-fit retrieval model on the TRAPPIST-1h spectrum corrected by Zhang et al. (2018) (top) and by Morris et al. (2018) (bottom). We omitted Rayleigh scattering opacity contributions from others species than  $H_2$  for clarity.

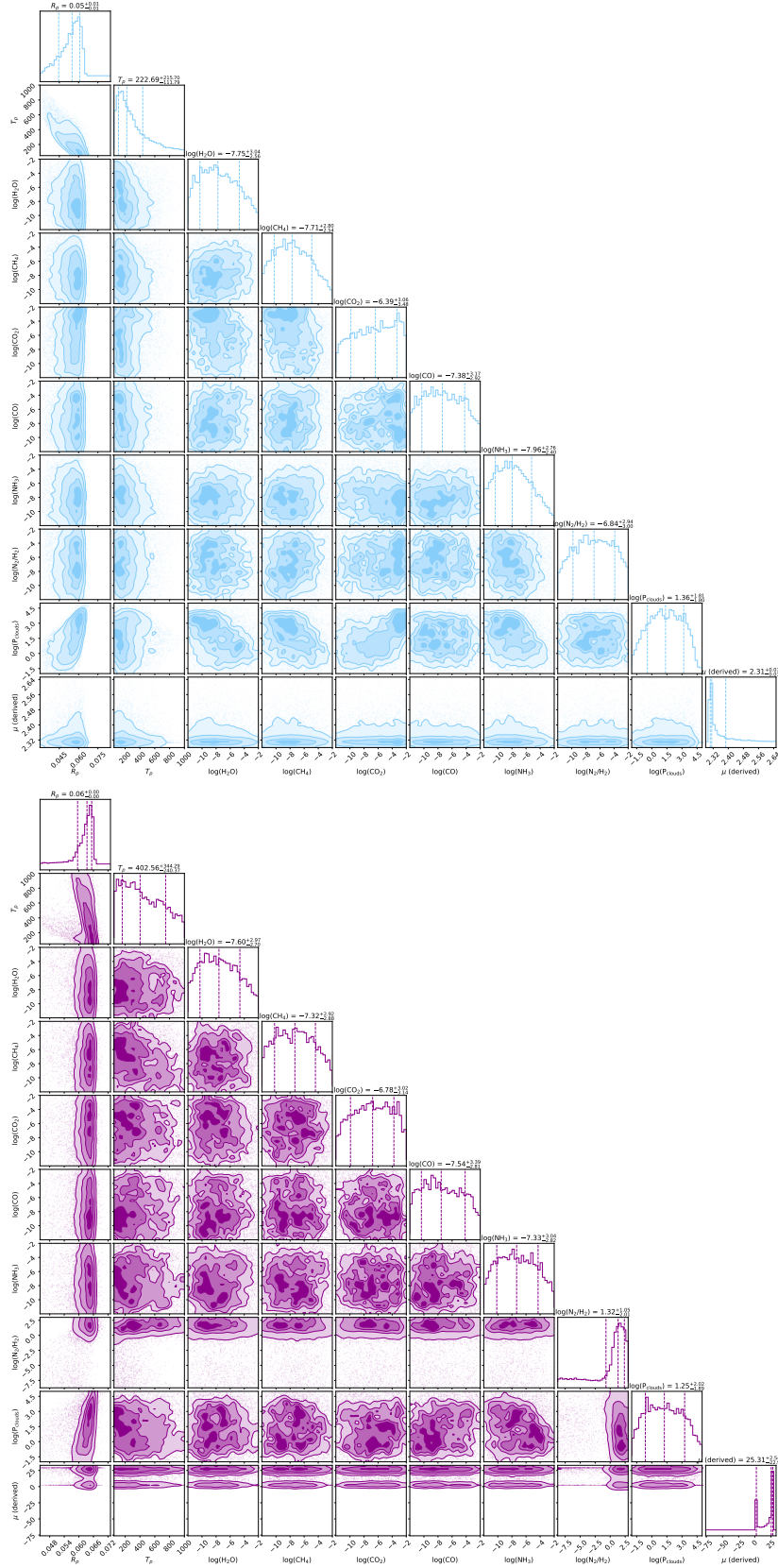


**Fig. B.7.** Posterior distributions for the primary atmospheric retrieval (top) and the secondary retrieval (bottom) on TRAPPIST-1b spectra corrected by the stellar contamination model of Zhang et al. (2018).

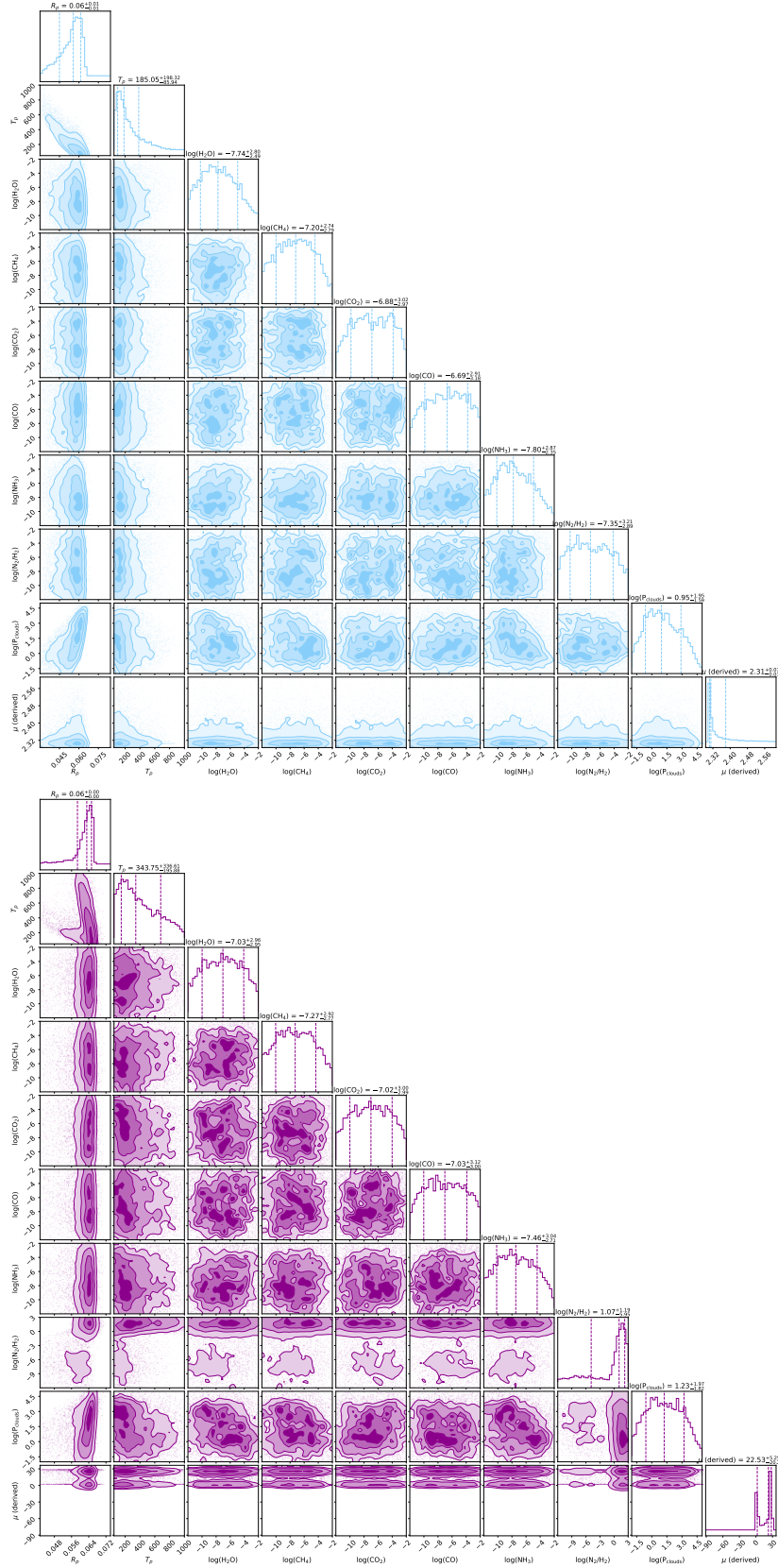


**Fig. B.8.** Posterior distributions for the primary atmospheric retrieval (top) and the secondary retrieval (bottom) on TRAPPIST-1h spectra corrected by the stellar contamination model of Wakeford et al. (2019).



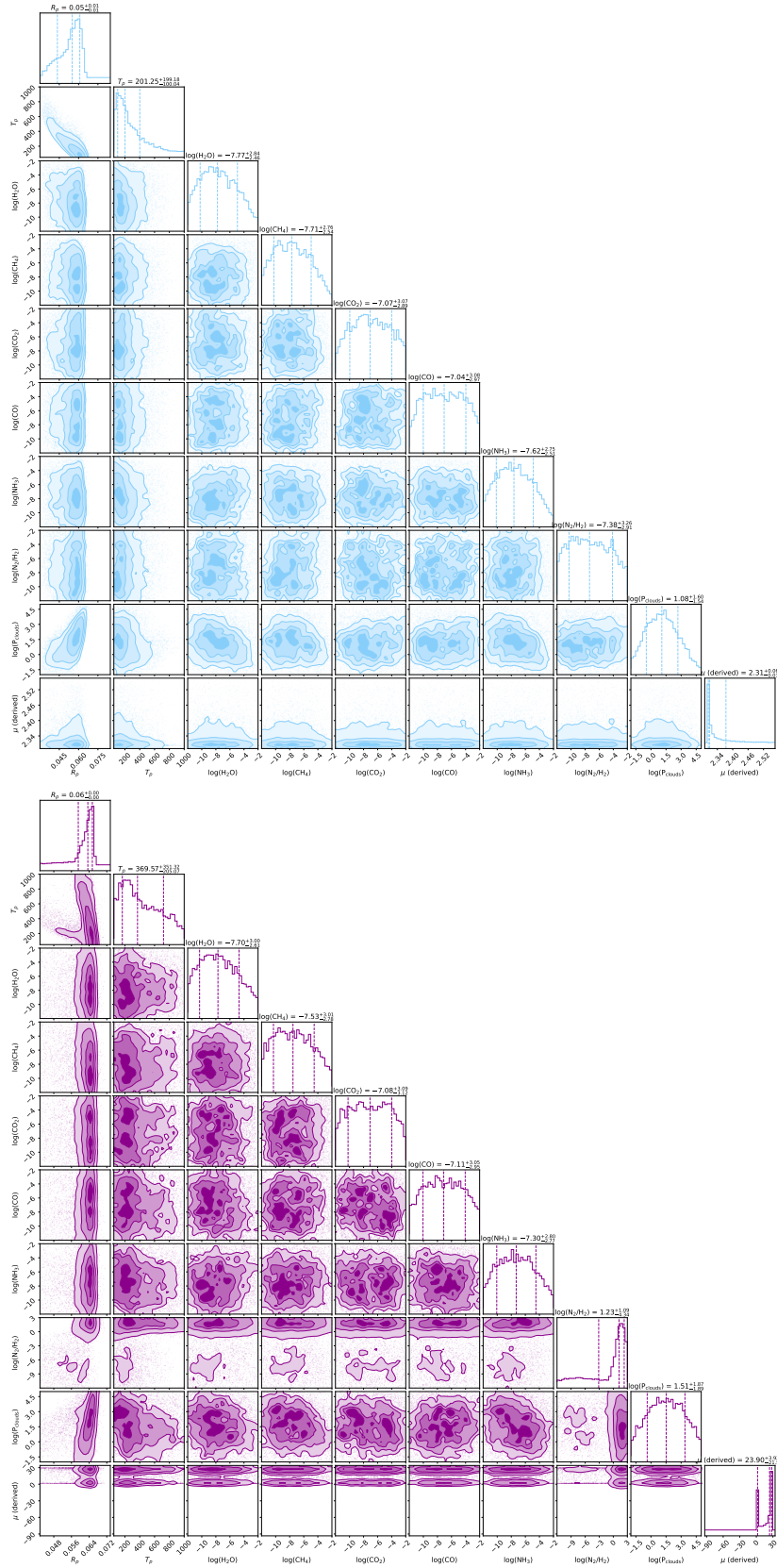


**Fig. B.9.** Posterior distributions for the primary atmospheric retrieval (top) and the secondary retrieval (bottom) on TRAPPIST-1h spectra corrected by the stellar contamination model of Morris et al. (2018).



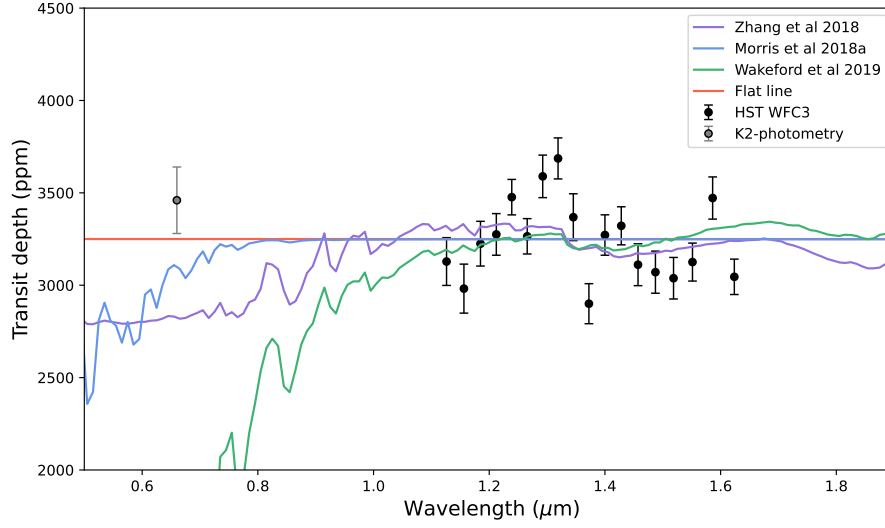


**Fig. B.10.** Best fit models to TRAPPIST-1 h HST/WFC3 G141 data (black) and K2 optical value (Luger et al. 2017a) (grey) from stellar contamination models based on Zhang et al. (2018), Wakeford et al. (2019), and Morris et al. (2018) .

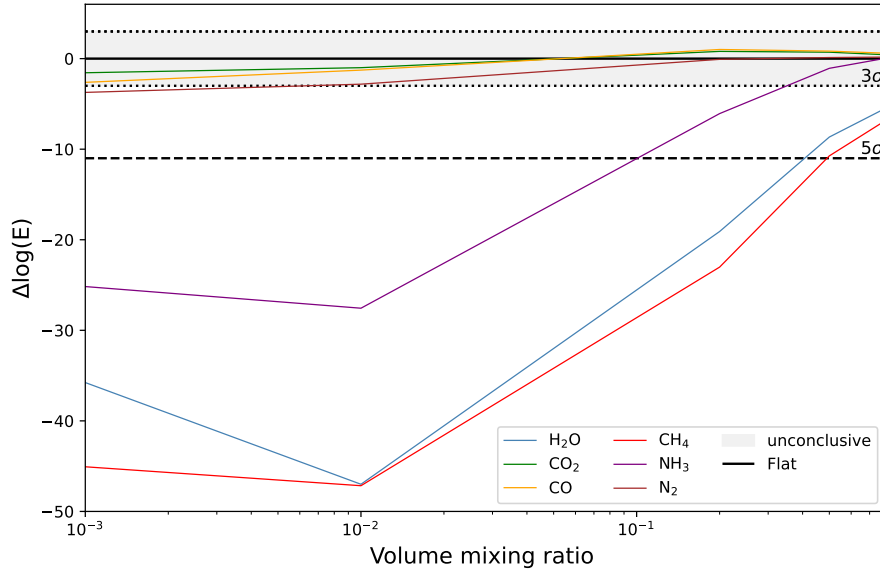


**Fig. B.11.** Comparison of the log evidence for a flat line to that of single molecule retrievals where the abundance of the molecule is fixed and no clouds were included. The shaded region represents the set of Bayes factor values for which it is not possible to conclude compared to a flat line, that is with absolute  $\Delta\log(E)$  below 3. Models below the dashed lines are strongly disfavoured compared to the flat line.